Development and Application of an Aero-Hydro-Servo-Elastic Coupling Framework for Analysis of Floating Offshore Wind Turbines

Yang YANG [a,b], Musa BASHIR [a,*], Constantine MICHAILIDES [c], Chun LI [b], Jin WANG [a]

[a.] Department of Maritime and Mechanical Engineering, Liverpool John Moores University, Liverpool, Byrom Street, L3 3AF, UK

[b.] School of Energy and Power Engineering, University of Shanghai for Science and Technology, Shanghai, 200093, P.R. China

[c.] Department of Civil Engineering and Geometrics, Cyprus University of Technology, Limassol, Saripolou 2-8, 3036, Cyprus

Abstract: In order to enhance simulation capabilities of existing numerical tools for the design of floating offshore wind turbines (FOWTs), this study has developed and implemented a coupling framework (F2A) that is capable of predicting nonlinear dynamics of a FOWT subjected to wind, wave and current loadings. F2A integrates all the advantages of FAST in efficiently examining aero-servo-elastic effects with all the numerical capabilities of AQWA (*e. g.* nonlinear hydrodynamics, mooring dynamics and material nonlinearity) for the dynamic analysis of a FOWT. The verification of F2A is carried out by comparing it with OpenFAST through the case study of a 5 MW wind turbine supported by the OC3-Hywind spar platform. The results show excellent agreements between F2A and OpenFAST in predicting dynamic responses of the blades, tower, platform and station-keeping system under both steady and turbulent winds combined with wave conditions. This implies that the simulation capabilities of FAST are well implemented within AQWA. Further advantages and capabilities of F2A in examining the dynamics of a FOWT are investigated via a case study of a multi-body platform concept connected by flexible elements. Some unique phenomena can only be observed from the results obtained using F2A as opposed to conventional tools. The results indicate that the newly-developed F2A coupling framework can be used for the analysis of FOWTs and it has been released to the public.

Keywords: Floating offshore wind turbines; AQWA; FAST; Aero-hydro-servo-elastic coupling framework;

* Corresponding author: m.b.bashir@ljmu.ac.uk

1 Introduction

Offshore wind is increasingly attracting attention to meet the growing demand of green energy development against environmental pollution caused by the consumption of fossil fuels. The 2019 annual wind report released by the International Energy Agency (IEA) indicates that the global offshore wind energy market has been expanding by nearly 30% per year since 2010, and the global offshore wind capacity is expecting an annual increase of more than 20 GW in the coming decade [1]. Development of floating offshore wind turbines (FOWTs) has been a research focus of both industrial and academic institutions due to its operational suitability in deeper sea areas where more abundant wind resources exist [2].

Implementation of a fully-coupled aero-hydro-servo-elastic model is crucial to producing reliable numerical predictions of dynamic responses for the design of FOWTs. The nonlinear coupling between aerodynamic and hydrodynamic loads, as well as free motion of the platform needs to be examined. A number of simulation tools were developed to address such problem. For instance, Cunff *et al.* [3-4] developed a fully-coupled aero-hydro-servo-elastic simulation tool named DeepLines for FOWTs. Aerodynamic loads were predicted by the blade element momentum theory (BEMT) method with the correction of a dynamic stall model. Finite element method (FEM) was used for the structural modelling of blades and tower. The diffraction and radiation problems of the floating platform were addressed through the Diodore solver that is a commercial hydrodynamic analysis software tool. Chen *et al.* [5] developed an aero-hydro-servo-elastic coupled tool (DARwind) for FOWTs based on Kane's kinetic method and the BEMT theory. The hydrodynamic load calculation was addressed through potential-flow theory. The DARwind tool was validated through comprehensive comparisons with experimental results.

In addition to these tools, Bladed and HAWC2 are the most well-known commercial software for design of wind turbines. Both of them employed the BEMT for calculation of

aerodynamic loads and the multi-body dynamic (MBD) method for structural modelling, resulting in a high efficiency when examining aero-elastic effects. Bladed and HAWC2 have been used to investigate coupled dynamic behavior of FOWTs [6-9]. FAST is another well-known aero-hydro-servo-elastic coupled simulation program for horizontal axis wind turbines. FAST predicts aerodynamic loads based on the BEMT and generalized wake model (GDW) in its AeroDyn module. The elasticity of the blades and tower was examined using the modal representation method. FAST was originally developed for design of onshore wind turbines. To make FAST capable of performing coupled analysis of FOWTs, Jonkman [10-11] developed a hydrodynamic module to consider diffraction and radiation effects of the floating platform. The mooring dynamics were examined using the quasi-static approach. FAST was used to conduct a comparative study of a 5 MW wind turbine supported by different platforms [12]. Due to its high efficiency and open source nature, FAST has been widely used in the initial design stage of a FOWT to conduct a large number of simulations [13-17].

Because of its open source nature, FAST was widely involved in the development of some fully-coupled tools by integrating it with another program. For example, Roddier [18] integrated FAST within a hydrodynamic analysis tool named TimeFloat for the fully-coupled modelling of the WindFloat concept. In another study by Kvittem *et al.* [19], a tool which incorporated AeroDyn within the nonlinear FEM software SIMO/REFLEX was used to establish a fully-coupled model of a 5 MW semi-submersible wind turbine. The validation of this tool was carried out by comparing with FAST and HAWC2. However, the comparison was made for a land-based wind turbine under steady-state conditions. Afterwards the effect of hydrodynamic modelling on the dynamic responses of the FOWT was investigated using the SIMO/REFLEX/AeroDyn tool. This tool was also used by Michailides *et al.* [20] for fully-coupled analysis of a semi-submersible FOWT combined with three flaps operating as wave energy converters. In addition, Shim [21] developed an interface to incorporate FAST with the

hydrodynamic analysis tool CHARM3D for the investigation of coupled dynamic responses of a 1.5 MW wind turbine supported by a TLP. The six degrees of freedom (DOFs) of the platform were solved in CHARM3D and then imported into FAST. Dynamic responses of the upper structures (*i.e*. the tower, nacelle, blades, *etc*.) were obtained in FAST by considering the positional changes of rotor and tower due to platform motions. Bae *et al.* [22-23] investigated coupling effects between wind and wave loadings of a 1.5 MW TLP wind turbine operating under different water depths using the same tool. The CHARM3D-FAST tool was also used to investigate the coupled dynamic behavior of a 5 MW spar wind turbine under survival conditions [24]. However, it should be noted that the CHARM3D-FAST tool did not consider velocity and acceleration of the platform in solving the equation of motion of the upper structures, implying that coupled dynamics of the upper structures including the blades and tower were not well examined. Furthermore, this tool has not been well validated yet.

In addition to the literature reviewed above, this study aims to develop a new aero-hydro-servo-elastic coupling framework (F2A) based on FAST and AQWA for dynamic analysis of FOWTs. AQWA [25] is a commonly-used commercial analysis tool capable of performing both frequency-domain and time-domain analysis of single and multi-body offshore structures. The hydrodynamic interaction between multiple floaters can be examined. Furthermore, AQWA has a powerful capability in addressing nonlinear dynamics of mooring lines subjected to an unexpected breakage in operational states. These advantages of AQWA in modelling of hydrodynamics and mooring dynamics will enhance the simulation capabilities of FAST for the design of FOWTs.

The implementation of the F2A coupling framework is achieved by modifying the source codes of FAST and the built-in dynamic link library (DLL) of AQWA. The displacement, velocity and acceleration of the platform obtained in AQWA are used in FAST subroutines to correct the kinematics of the wind turbine's upper structures when solving their equations of

motion. The tower-base loads that represent the complicated aero-servo-elastic effects of the wind turbine are imported into AQWA for solving the moored platform's responses. Details of the development of F2A are presented in Section 2. Following this, comprehensive comparisons against OpenFAST, an updated version of FAST, are made to validate the accuracy and credibility of F2A in performing a fully-coupled analysis of a FOWT. The coupled dynamic responses of the NREL 5 MW wind turbine supported by the OC3-Hywind spar platform under steady-states and turbulent inflow conditions are presented and discussed. A case study of a 10 MW FOWT multi-body platform is presented in Section 4, which demonstrates the superiority of F2A in capturing the dynamic effects of a multi-body platform. Furthermore, the case study demonstrates how the limitations of the commonly-used tool, FAST, are addressed. The main conclusions of this study are presented in Section 5. Information on the public release of F2A is given in Appendix A.

2 Methodologies for the development of F2A

F2A integrates aero-servo-elastic simulation capability of FAST within AQWA by implementing a new fully-coupled method through the built-in DLL of AQWA that is used to calculate external forces in a time-domain analysis. The subsequent sections briefly describe the basic theories used in FAST and AQWA for structural modelling and environmental load predictions, as well as implementation details of F2A.

2.1 Aerodynamic and structural modelling in FAST

FAST is an aero-hydro-servo-elastic fully-coupled simulation tool developed by NREL for the design of horizontal axis wind turbines. The basic version of FAST (version 7.03) [26] consists of AeroDyn, ElastDyn, HydroDyn and ServoDyn modules. The modules are coupled with each other in a time-domain analysis. However, the HydroDyn module is not involved in

the development of F2A since the hydrodynamic loads are predicted by AQWA.

In the AeroDyn module, the BEMT is used to calculate the aerodynamic loads acting on the blades based on the lift and drag coefficients of the sectional airfoils and local induction velocities that are determined using the GDW model. Fig. 1 illustrates the aerodynamic forces of an arbitrary blade element with a length of d*r*. In Fig. 1, Ω is the rotor speed. *r* is the local radius of the blade element. *V* and *W* denote the inflow and absolute speed, respectively. *a* and *b* are axial and tangential induction coefficients, respectively. α , β and ϕ are the angles of attack, twist and inflow, respectively. *L* and *D* are the lift and drag forces, respectively.

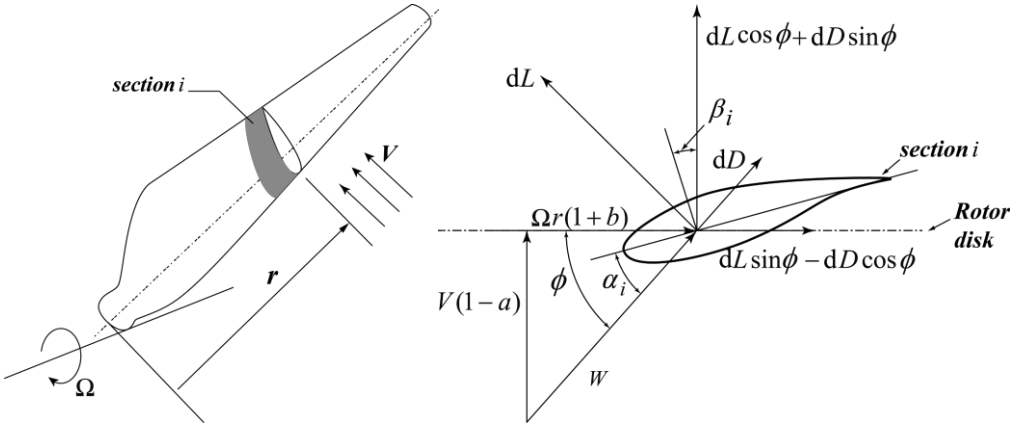

Fig. 1: Velocities and aerodynamic forces of an arbitrary blade section (source [27])

The angle of attack of the local section is determined based on the induction velocities. The aerodynamic coefficients of the corresponding section are then obtained to calculate the thrust and torque using Eq. (1) and Eq. (2):

$$\mathrm{d}T = \frac{1}{2}\rho W^2 c(C_l \cos\phi + C_d \sin\phi)\mathrm{d}r \tag{1}$$

$$\mathrm{d}M = \frac{1}{2}\rho W^2 c(C_l \sin\phi - C_d \cos\phi) r\mathrm{d}r \tag{2}$$

where C_l and C_d are respectively the lift and drag coefficients of the sectional airfoil. The Beddoes-Leishman dynamic stall model is used to correct the aerodynamic coefficients under unsteady conditions. *c* is the chord length of the blade element.

Further details on the theories used in AeroDyn for predicting aerodynamic loads acting on the blades can be found in [28-29]. Aerodynamic loads calculated in the AeroDyn module are imported into the ElastDyn to solve the equations of motion of the wind turbine. The Kane's kinetic method was used to establish the equation of motion as denoted in Eq. (3)

$$\boldsymbol{F}_r^* + \boldsymbol{F}_r = 0 \tag{3}$$

where $\boldsymbol{F}_r^*$ is the generalized inertia force vector and $\boldsymbol{F}_r$ is the generalized active force vector.

The wind turbine was modelled as a multi-body system consisting of rigid bodies and flexible bodies. The hub and nacelle were treated as rigid bodies. The tower and blades were modelled as flexible bodies. The generalized inertia force of a rigid body can be represented using the same formula. For instance, the generalized inertia force of the nacelle $\boldsymbol{F}_{r,\mathrm{Nac}}^*$ is derived as:

$$\boldsymbol{F}_{r,\mathrm{Nac}}^* = \sum_{i=1}^{N} \boldsymbol{v}_{i,\mathrm{Nac}} (-m_{\mathrm{Nac}} \cdot \boldsymbol{a}_{\mathrm{Nac}}) + \boldsymbol{\omega}_i (-\dot{\boldsymbol{H}}_{\mathrm{Nac}}) \tag{4}$$

where N is the number of total examined DOFs of the wind turbine. $\boldsymbol{v}_{i,\mathrm{Nac}}$ is the partial velocity of the nacelle contributed by the i^{th} DOF of the wind turbine. m_{Nac} and $\boldsymbol{a}_{\mathrm{Nac}}$ are respectively the mass and acceleration of the nacelle. $\boldsymbol{\omega}_i$ is the partial angular velocity of the nacelle contributed by the i^{th} DOF of the wind turbine. $\dot{\boldsymbol{H}}_{\mathrm{Nac}}$ is the time derivative of angular momentum of the nacelle about its mass center.

The generalized inertia force of the hub can be represented using a similar formula to Eq. (4). The generalized inertia force of the tower $\boldsymbol{F}_{r,\mathrm{Twr}}^*$ is denoted as:

$$\boldsymbol{F}_{r,\mathrm{Twr}}^* = \sum_{i=1}^{N} \int_0^{H_0} \rho_{\mathrm{Twr}}(h) \cdot \boldsymbol{v}_{i,\mathrm{Twr}}(h) \cdot \boldsymbol{a}_{\mathrm{Twr}}(h) \cdot \mathrm{d}h \tag{5}$$

where H_0 is the tower length. $\rho_{\mathrm{Twr}}(h)$ is the mass of tower per unit length. $\boldsymbol{v}_{i,\mathrm{Twr}}(h)$ is the partial velocity of the local tower section contributed by the i^{th} DOF of the wind turbine. $\boldsymbol{a}_{\mathrm{Twr}}(h)$ is the acceleration of the local tower section.

The generalized inertia force corresponding to a blade can be denoted in a similar formula to Eq. (5). The generalized active forces are composed of aerodynamic load, elastic restoring force and other environmental loads as denoted in Eq. (6).

$$F_r = F_{r,\text{aero}} + F_{r,\text{elastic}} + F_{r,\text{grav}} + F_{r,\text{damp}} \tag{6}$$

The generalized active aerodynamic force acting on a blade $F_{r,\text{aero}}$ is denoted as:

$$F_{r,\text{aero}} = \sum_{i=1}^{N} \int_0^{R-R_{\text{hub}}} v_{i,\text{Bld}}(r) \cdot F_{\text{aero}}(r) \cdot \mathrm{d}r \tag{7}$$

where R and R_{hub} are the radii of the rotor and hub, respectively. $v_{i,\text{Bld}}(r)$ is the partial velocity of the local blade section contributed by the i^{th} DOF of the wind turbine. $F_{\text{aero}}(r)$ is the total force acting on the local blade section.

An exhaustive development of all these local generalized active forces is beyond the scope of this study. More details on the equations of motion established in FAST can be found in [30-31]. A fourth-order Adams-Beshforth-Mounton predictor-corrector method is used to determine the accelerations in the time-marching solution process.

2.2 Mooring dynamics

The finite element method is used to model the mooring lines in order to examine the dynamic effects of mooring lines. Each mooring line is discretized into a number of finite elements where the mass of each element is concentrated into a corresponding node. Fig. 2 presents a schematic diagram of the dynamic model of a mooring line. In the figure, S_j is the unstretched length between the anchor and the j^{th}-node of the mooring line, D_e is the diameter of the local segment of the mooring line.

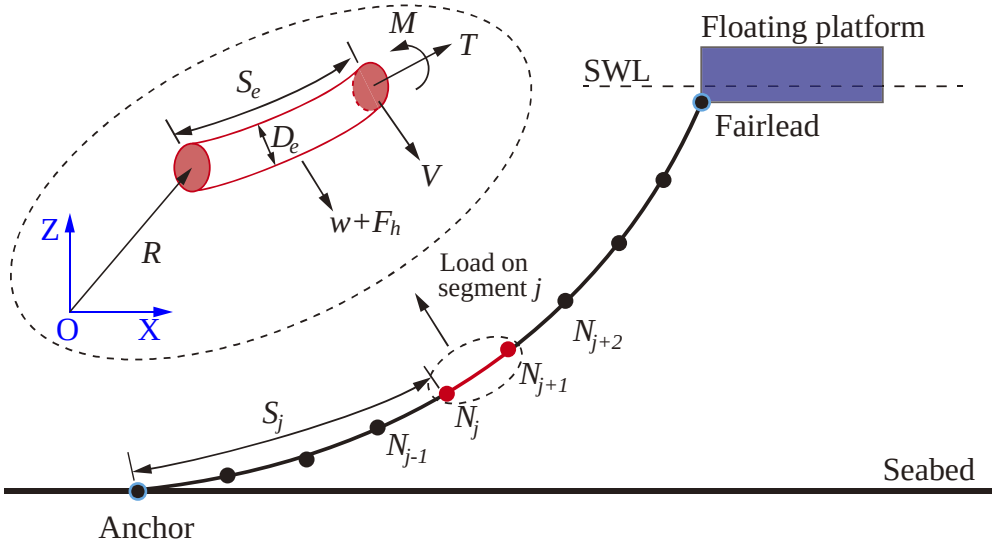

Fig. 2: Schematic diagram of the dynamic model of a mooring line

Each of the mooring lines is modelled as a chain of Morison-type elements subjected to various external forces. The equation of motion of an arbitrary element of the mooring line is presented as follows [32]:

$$\begin{cases} \dfrac{\partial \mathbf{T}}{\partial S_e} + \dfrac{\partial \mathbf{V}}{\partial S_e} + \boldsymbol{w} + \boldsymbol{F}_h = m_e \dfrac{\partial^2 \mathbf{R}}{\partial t^2} \\ \dfrac{\partial \mathbf{M}}{\partial S_e} + \dfrac{\partial \mathbf{R}}{\partial S_e} \times \mathbf{V} = -\mathbf{q} \end{cases} \tag{8}$$

where **T** and **V** are, respectively, the tension force and shear force vectors at the first node of the element; **R** is the position vector of the first node of the cable element; S_e is the unstretched length of the element; $\boldsymbol{w}$ and $\boldsymbol{F}_h$ are, respectively, the weight and hydrodynamic load vectors per unit length of the element; m_e is the mass per unit length. **M** is the bending moment vector at the first node of the element; and **q** is the distributed moment load per unit length of the element.

The bending moment and tension are denoted as follows:

$$\begin{cases} \mathbf{M}=EI\cdot\dfrac{\partial\mathbf{R}}{\partial S_e}\times\dfrac{\partial^2\mathbf{R}}{\partial S_e^2} \\ \mathbf{T}=EA\cdot\varepsilon \end{cases} \tag{9}$$

where EI and EA are the bending stiffness and axial stiffness of the mooring line, respectively.

In order to ensure a unique solution to Eq. (8), pinned connection boundary conditions are imposed at the top and bottom ends, as given in Eq. (10).

$$\begin{cases} \mathbf{R}(0)=\mathbf{P}_{\text{bot}},\mathbf{R}(L)=\mathbf{P}_{\text{top}} \\ \dfrac{\partial^2\mathbf{R}(0)}{\partial S_e^2}=\mathbf{0},\dfrac{\partial^2\mathbf{R}(L)}{\partial S_e^2}=\mathbf{0} \end{cases} \tag{10}$$

where $\mathbf{P}_{\text{bot}}$ and $\mathbf{P}_{\text{top}}$ are the position vectors of attachment points of the mooring line; and L is the unstretched length of the mooring line.

It is noted that the solution of the mooring tension is fully coupled with platform motions. This means that the effects of the mooring mass, drag forces, inline elastic tension and bending moment are examined.

2.3 Development of the coupling framework

Although the baseline version of AQWA is incapable of predicting aerodynamic load and structural responses of FOWTs, it accepts external forces calculated through the *user_force.dll* for a time-domain analysis. In order to make AQWA capable of performing fully-coupled analysis of FOWTs, this study has developed and implemented a coupling framework presented in Fig. 3 to integrate some simulation capabilities of FAST within AQWA. Therefore, the coupling framework is so-called “FAST2AQWA”, simplified as F2A.

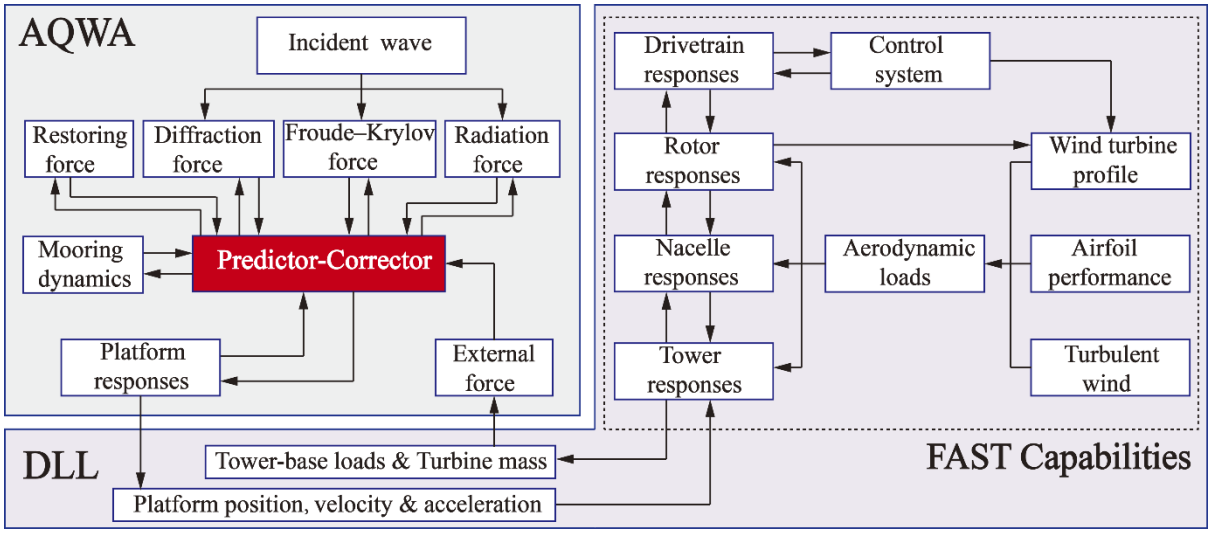

Fig. 3: Coupling framework between AQWA and FAST

The coupling between AQWA and FAST is achieved through modifications on the source codes of the *user_force.dll* and FAST subroutines. The relevant simulation capabilities of FAST are fully implemented within the DLL which can be invoked by AQWA during a time-domain analysis. As can be seen from Fig. 3, position, velocity and acceleration of the platform obtained in AQWA will be used to determine the dynamic responses of the upper structures of the wind turbine. Tower-base loads calculated by FAST subroutines are passed into AQWA as external forces for solving the following equation of motion of the platform:

$$\boldsymbol{M}\ddot{X}(t)+\boldsymbol{C}\dot{X}(t)+\boldsymbol{K}X(t)+\int_0^t h(t-\tau)\ddot{X}(\tau)\mathrm{d}\tau=\boldsymbol{F}(t) \tag{11}$$

where $\boldsymbol{M}$ is the mass matrix assembled by the inertial and added masses. $\ddot{X}(t)$ is the unknown acceleration vector at the time t. $\boldsymbol{F}(t)$ is the total external force vector including the hydrodynamic and aerodynamic loads. $\boldsymbol{C}$ and $\boldsymbol{K}$ are respectively the assembled damping and stiffness matrices; $h(t)$ is the acceleration impulse function matrix used to examine the radiation memory effects as defined in Eq. (12).

$$\boldsymbol{h}(t)=\frac{2}{\pi}\int_0^\infty \boldsymbol{B}(\omega)\frac{\sin(\omega t)}{\omega}\mathrm{d}\omega \tag{12}$$

where $\boldsymbol{B}(\omega)$ is the radiation damping corresponding to the wave frequency of ω.

The equation of motion of the wind turbine described in Eq. (3) and the equation of motion of the floating platform derived in Eq. (11) are solved independently in the DLL and AQWA program, respectively. The solutions of these equations are coupled with each other. AQWA uses a predictor-corrector algorithm in the time-marching solution process. The DLL will be invoked twice during each time-step in a simulation. Fig. 4 presents the process of a time-domain analysis performed using F2A. It is noted that the dynamic responses of the upper structures predicted in the DLL are influenced by the platform responses obtained in AQWA and vice versa.

For a simulation with a duration of $T_{\max}$ and a time-step of Δt, hydrodynamic loads and mooring restoring forces are calculated in the AQWA program based on the initialized platform responses. The DLL that contains simulation capabilities of FAST is invoked to obtain tower-base loads based on the platform responses at current time (t). These results are used to predict the platform responses at the next time step ($t + \Delta t$) after applying an appropriate transformation to unify the coordinate system. Then, the hydrodynamic loads and mooring restoring forces acting on the platform will be calculated once again. Simultaneously, the tower-base loads will be calculated using the DLL. Afterwards, platform responses at the next time-step ($t + \Delta t$) will be determined in AQWA. The processes are repeated until the simulation is successfully terminated.

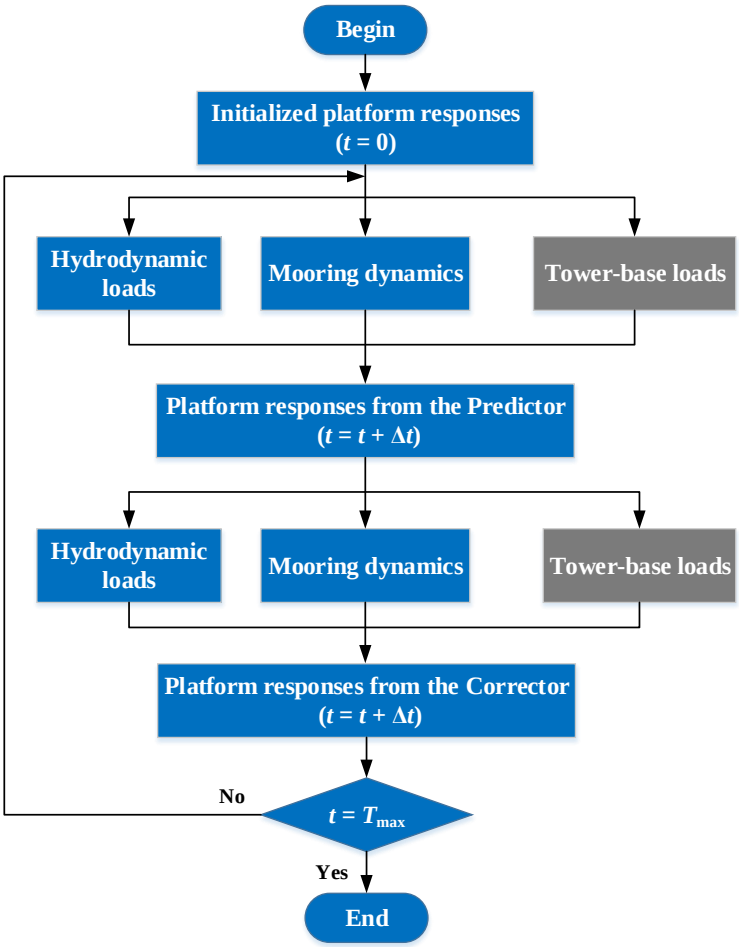

Fig. 4: Process of a simulation conducted using F2A

In the calculation of tower-base loads, the equation of motion of the wind turbine excluding the platform as denoted in Eq. (5) is solved. The kinematics of the upper structures (*i.e.* blades, tower, nacelle, *etc.*) are influenced by the position, velocity and acceleration of the platform. It is apparent that dynamic responses of the upper structures and platform are coupled with each other through the developed coupling framework F2A.

It is noted that the results produced by AQWA and the DLL are referred with different coordinate systems. To be more specific, the platform responses predicted by AQWA represent the position, velocity and acceleration of the platform's mass center that are referred with the inertial coordinate system. However, the kinematics of the upper structures are corrected based on the platform responses that are referred with its local coordinate system. Similarly, the load

vector that will be passed into AQWA acts at the tower-base is referred with respect to the platform's local coordinate system, but the external force used in Eq. (11) acts at the platform's mass center and is referred with the inertial coordinate system. Therefore, the results directly obtained by AQWA and the DLL require transformations before passing into each other.

Firstly, a transformation needs to be made on the platform position and velocity vectors obtained in AQWA. The transformation matrix $\mathbf{T}_{\text{mat}}$ [11] is used to correct the platform position vector as presented in Eq. (23).

$$\begin{bmatrix} x \\ y \\ z \end{bmatrix} = \begin{bmatrix} \dfrac{\theta_1^2\sqrt{1+s}+\theta_2^2+\theta_3^2}{s\sqrt{1+s}} & \dfrac{\theta_3 s+\theta_1\theta_2(\sqrt{1+s}-1)}{s\sqrt{1+s}} & \dfrac{-\theta_2 s+\theta_1\theta_3(\sqrt{1+s}-1)}{s\sqrt{1+s}} \\ \dfrac{-\theta_3 s+\theta_1\theta_2(\sqrt{1+s}-1)}{s\sqrt{1+s}} & \dfrac{\theta_2^2\sqrt{1+s}+\theta_1^2+\theta_3^2}{s\sqrt{1+s}} & \dfrac{\theta_1 s+\theta_2\theta_3(\sqrt{1+s}-1)}{s\sqrt{1+s}} \\ \dfrac{\theta_2 s+\theta_1\theta_3(\sqrt{1+s}-1)}{s\sqrt{1+s}} & \dfrac{-\theta_1 s+\theta_2\theta_3(\sqrt{1+s}-1)}{s\sqrt{1+s}} & \dfrac{\theta_3^2\sqrt{1+s}+\theta_1^2+\theta_2^2}{s\sqrt{1+s}} \end{bmatrix} \begin{bmatrix} X \\ Y \\ Z \end{bmatrix} \tag{13}$$

where $[x, y, z]^{\mathrm{T}}$ is the corrected position vector that will be passed into FAST. $[\mathrm{X}, Y, Z]^{\mathrm{T}}$ is the position vector obtained in AQWA. θ_1, θ_2 and θ_3 are the roll, pitch and yaw motions of the platform, respectively; s is the sum of the squares of the rotations, *i.e.* $\theta_1^2+\theta_2^2+\theta_3^2$.

The translational velocities of the platform shall be corrected accordingly before passing into FAST subroutines. When the platform reference point defined in FAST is the origin of the inertial coordinate system, *i.e.* (0, 0, 0), the translational velocities of the platform are corrected through Eq. (14).

$$\mathbf{V} = \mathbf{U} - \mathbf{T}_{\text{mat}} \cdot \mathbf{CoG} \times \boldsymbol{\omega} \tag{14}$$

where $\mathbf{V}$ is the translational velocity vector used in FAST. $\mathbf{U}$ and $\boldsymbol{\omega}$ are, respectively, the translational and rotational velocity vectors of the platform obtained in AQWA. $\mathbf{CoG}$ is the position vector from the reference point to the center of mass of the platform.

It is noted that FAST adopts a predictor-corrector algorithm to numerically solve the equations of motion in time-domain, the acceleration vector calculated in the predictor stage

will be used in the corrector stage for the final solution. Therefore, the platform acceleration vector is essential to the time-marching process in FAST for updating the kinematics of the entire wind turbine. However, the platform acceleration is unavailable until the completion of solving the equation of motion in AQWA at the current time-step. Therefore, the platform acceleration will be estimated numerically in the DLL based on the velocities at the last time-step and current time-step.

Similarly, the load vector obtained in FAST subroutines will be corrected before passing it into AQWA. The expressions presented in Eq. (15) and Eq. (16) are used to convert the translational and rotational loads, respectively, when the tower-base is the origin of the inertial coordinate system.

$$\mathbf{F}_{\mathrm{AQWA}} = \mathbf{T}_{\mathrm{mat}}^{-1} \cdot \mathbf{F}_{\mathrm{FAST}} \tag{15}$$

$$\mathbf{M}_{\mathrm{AQWA}} = \mathbf{T}_{\mathrm{mat}}^{-1} \cdot (\mathbf{M}_{\mathrm{FAST}} - \mathbf{CoG} \times \mathbf{F}_{\mathrm{FAST}}) \tag{16}$$

where $\mathbf{F}_{\mathrm{AQWA}}$ and $\mathbf{F}_{\mathrm{FAST}}$ are the translational force vectors in AQWA and FAST, respectively. $\mathbf{T}_{\mathrm{mat}}^{-1}$ is the inverse matrix of $\mathbf{T}_{\mathrm{mat}}$. $\mathbf{M}_{\mathrm{AQWA}}$ is the moment vector at the platform mass center with respect to the inertial coordinate system in AQWA. $\mathbf{M}_{\mathrm{FAST}}$ is the moment vector acting at the tower-base obtained in FAST with respect to the tower-base local coordinate system.

3 Validation of the coupling framework

The validation of the F2A coupling framework is carried out by comparing it with OpenFAST. The extensively-used OC3-Hywind spar platform is employed as the validation model. The subsequent sections present a brief description of the spar model and detailed comparisons of the responses in time-domain for both steady and turbulent wind conditions.

3.1 OC3-Hywind spar model

In 2010, the Hywind spar concept originally developed by Statoil was modified to accommodate the NREL 5 MW wind turbine [34] for utilization in the offshore code comparison collaboration (OC3) project [35]. The so-called "OC3-Hywind" platform has been extensively used in the design and analysis of FOWTs due to its structural simplicity, modelling suitability and commercial viability. Therefore, the OC3-Hywind spar concept is chosen as the case study model to validate the accuracy and credibility of F2A. The spar model accommodated for the NREL 5 MW wind turbine has a total draft of 120 m and a mass including ballast of 7.466×10^6 kg. The design water-depth is 320 m. Table 1 summarizes main specifications of the spar model and the mooring system. Fig. 4 presents the spar model adopted for the NREL 5 MW wind turbine.

Table 1: Main specifications of the OC-3 Hywind spar platform and the mooring system

Property	**Value**	**Unit**
Platform mass	7,466,330	(kg)
Undisplaced volume of water	8029.21	(m^3)
Center of gravity (CoG) below SWL	89.9155	(m)
Platform roll inertia about CoG	4,229,230,000	($kg{\cdot}m^2$)
Platform pitch inertia about CoG	4,229,230,000	($kg{\cdot}m^2$)
Platform yaw inertia about CoG	164,230,000	($kg{\cdot}m^2$)
Additional yaw stiffness	98,340,000	Nm/rad
Number of mooring lines	3	(-)
Depth to anchors below SWL	320	(m)
Depth to fairleads below SWL	70.0	(m)
Radius to anchors	853.87	(m)
Radius to fairleads	5.2	(m)
Upstretched length of mooring lines	902.2	(m)
Mass density of mooring lines	77.7066	(kg/m)
Diameter of mooring lines	0.09	(m)
Equivalent weight in water	698.094	(N/m)
Extensional stiffness of mooring lines	384,243,000	(N)

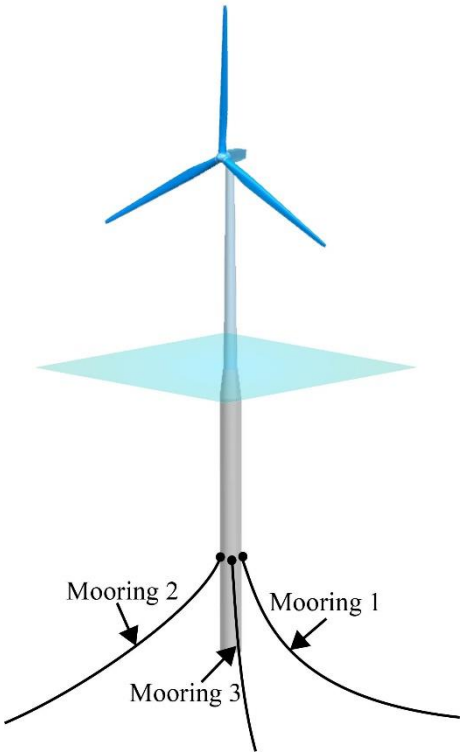

Fig. 5： NREL5 MW wind turbine supported by the OC3-Hywind spar platform

3.2 Time-domain validation against OpenFAST

The validation in time-domain is carried out by comparing it with OpenFAST (an updated version of FAST). The MoorDyn module is used to examine the dynamic effects of the mooring lines in OpenFAST. The hydrodynamic coefficients used in HydroDyn module of OpenFAST for the calculation of hydrodynamic loads are obtained using WAMIT. The time-domain comparisons are carried out for both steady and turbulent wind conditions. Since the procedure of generating an irregular wave in OpenFAST and AQWA is distinct, the waves examined in the time-domain validation are regular types to avoid any interference that might be caused by the difference of incident wave kinematics. Nonetheless, the 3-D turbulent wind field generated using TurbSim based on the Kaimal spectrum is the same for both AQWA and OpenFAST. The same controller is used to adjust blade-pitch and generator torque for normal power production.

3.2.1 Sensitivity analysis of simulation time step

In order to avoid any potential convergence issues and other adverse effects from a large time step, a sensitivity analysis of the time step is carried out. The time step in a time-domain analysis in AQWA is allowed to be different from the time step in solving the structural dynamics through the DLL. The platform motions and mooring tensions of the NREL 5MW spar wind turbine under turbulent wind condition are obtained by conducting a series of simulations with different time steps. Fig. 6 presents the time-varying platform pitch motion obtained using F2A with different time steps. The relevant statistical results of the time step sensitivity analysis are presented in Fig. 7. The time step for solving structural dynamics is fixed at 0.005 s that is sufficiently small to avoid a numerical instability. It is observed that the difference between the results obtained from the simulations with different time steps is negligible. The maximum platform pitch motions are 7.079 degrees and 7.092 degrees for time steps of 0.1 s and 0.01 s, respectively, with a relative error of 0.17%. The corresponding relative errors for the minimum and mean values are smaller than 0.1%. This means that the platform motion is independent of the time step when the time step is smaller than 0.1 s. Therefore, the time step of 0.1 s is adopted for the remaining simulations conducted in this study.

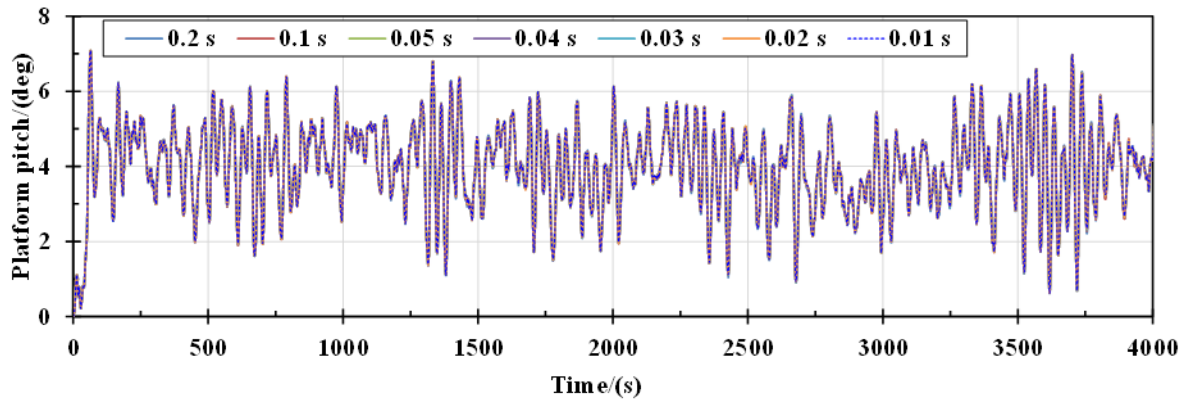

Fig. 6: Platform pitch motions under different time steps

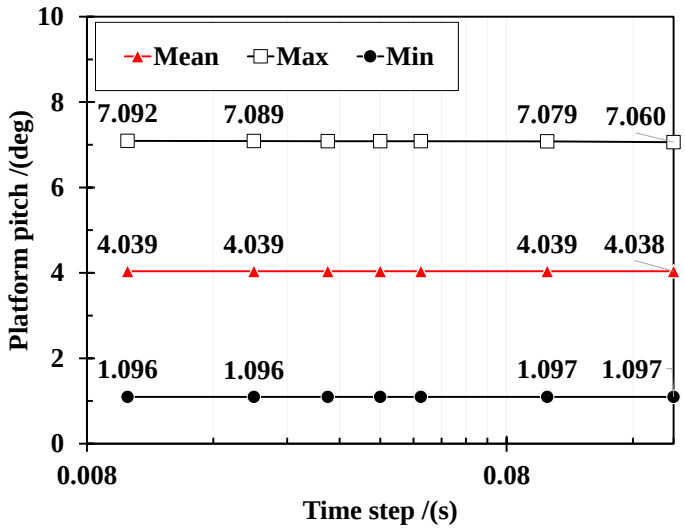

Fig. 7: Minimum, mean and maximum platform pitch motions under different time steps

3.2.2 Wave-only condition

The added mass, radiation damping and excitation force of the platform used in OpenFAST to calculate the hydrodynamic loads are obtained using WAMIT, while the corresponding hydrodynamic coefficients used in F2A are calculated by AQWA. As demanded by HydroDyn in OpenFAST, the vertical center of mass is set to zero to avoid double counting of the pitch/roll restoring force. Consequently, the excitation pitch/roll force obtained through WAMIT is smaller than that obtained using AQWA as shown in Fig. 8. The excitation force obtained using WAMIT agrees well with the results from AQWA when the vertical center of mass is set to zero in these two tools. However, when the center of mass is appropriately set in AQWA to be consistent with the reality, the excitation force is larger than the result used in OpenFAST. In addition, WAMIT employs the Rankine theory to solve the potentials of velocity and pressure in frequency-domain, while AQWA is based on Green's theorem to obtain the solutions. The different frequency-domain solutions used in OpenFAST and F2A are anticipated to produce discrepancies on the platform motions.

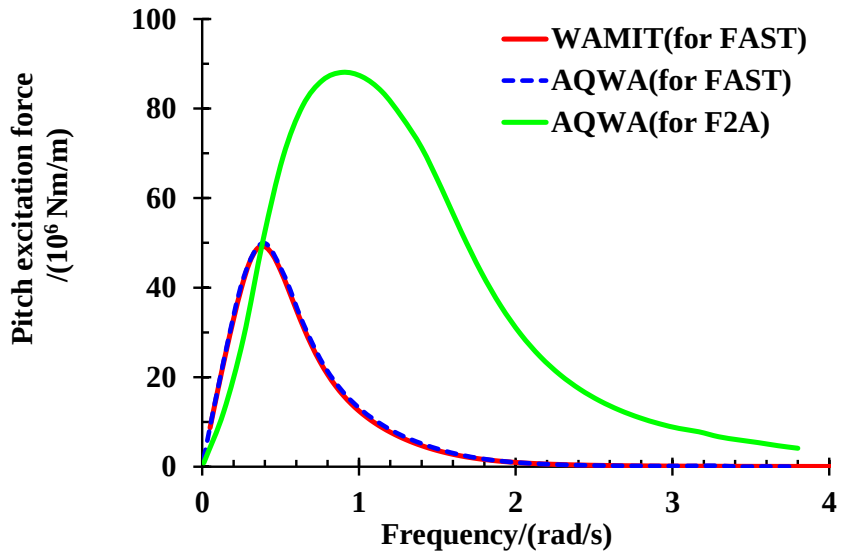

Fig. 8: Non-dimensional pitch excitation force coefficient obtained using WAMIT and AQWA

In order to evaluate the hydrodynamic loads induced discrepancy, the platform motions under a regular wave condition are obtained using OpenFAST and AQWA and presented in Fig. 9. The wave height and period are 1.94 m and 5.01 s, respectively. It is found that the results from OpenFAST and AQWA follow the same trend. The periods of the platform motion variations are identical. The platform motions obtained using AQWA are slightly larger than those results from OpenFAST as expected. More specifically, the platform surge and pitch predicted by AQWA are respectively around 0.1 m and 0.1 degree larger than the results obtained using OpenFAST. The difference in the heave motion is relatively small.

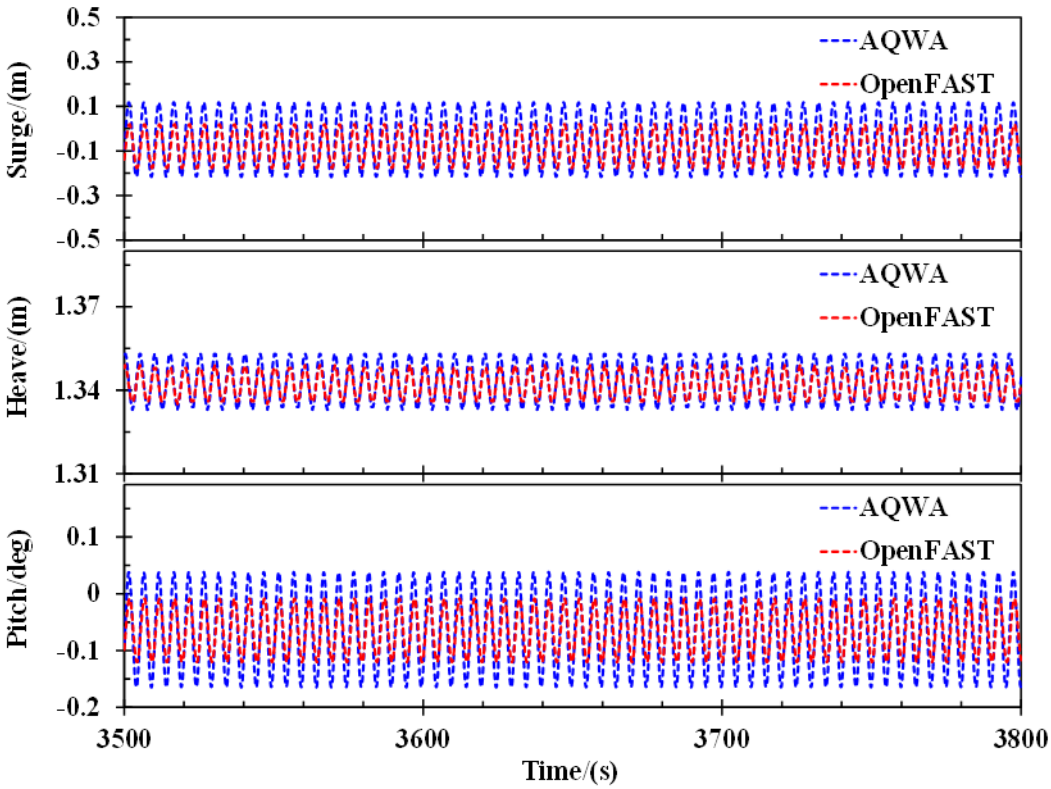

Fig. 9: Platform motions under the wave-only condition

3.2.3 Steady wind conditions

The comparisons of steady wind conditions are carried out to validate the accuracy of the F2A in evaluating dynamic responses of the FOWT within its operation wind speed range. Based on the observation met-ocean data of a specific site off the northern coast of Scotland [36], the design load cases (DLCs) presented in Table 2 are defined. The wind speed is assumed to be a constant for each DLC and the regular waves are generated using the Airy wave theory. Each of the simulations has a duration of 1500 s and a time step of 0.005 s. The statistical responses presented below are evaluated based on the results between 500 s and 1500 s.

Table 2: DLCs for the validation of steady wind and regular wave conditions

ID of DLCs	Wind Speed (m/s)	Wave height (m)	Wave period (s)
1	4.0	1.6146	3.4985
2	5.0	1.6356	3.5989
3	6.0	1.6660	3.7746

4	7.0	1.6987	3.9842
5	8.0	1.8037	4.2657
6	9.0	1.9027	4.6698
7	10.0	2.0125	4.8954
8	11.0	2.1155	5.2555
9	12.0	2.2237	5.5570
10	13.0	2.3660	5.9987
11	14.0	2.4570	6.3366
12	15.0	2.5570	6.5657
13	16.0	2.6588	6.8895
14	17.0	2.7985	6.9955
15	18.0	2.9585	7.1203
16	19.0	3.0125	7.2335
17	20.0	3.1547	7.4570
18	21.0	3.3357	7.7785
19	22.0	3.4587	8.0225
20	23.0	3.6846	8.2266
21	24.0	3.8975	8.5650
22	25.0	4.0257	8.8897

It is found that each simulation performed using F2A takes 20 minutes on a laptop with the CPU of Intel i5-4210U @1.70GHz. The computational efficiency is much higher than that of OpenFAST v2.3 which takes 46 minutes to complete a simulation with the same length using the same laptop. The reason is that more modules are integrated within OpenFAST. As a result, more processes are required for the data mapping and error checks. In addition, AQWA allows for running the simulation in parallel over multiple processors but OpenFAST can only invoke one processor per simulation.

The average values of controller parameters and rotor thrust under the DLCs listed in Table 2 are presented in Fig. 10. The error-bar corresponds to the standard deviation. It can be seen that the difference between the blade-pitch angles calculated by OpenFAST and F2A is negligible for each of the examined DLCs. For the rotor speed and electric power, slight differences can be observed in condition with a wind speed of 10 m/s. Rotor thrusts predicted using F2A agree well with the results obtained by OpenFAST for all wind conditions. Minor discrepancies exist under the wind scenarios close to the rated condition (11.4 m/s). For the over-rated conditions, the standard deviations of rotor speed and thrust calculated by F2A are

in line with those predicted by OpenFAST. The comparisons imply that F2A has a high accuracy in handling the servo-control and predicting rotor dynamics of the FOWT under steady wind conditions.

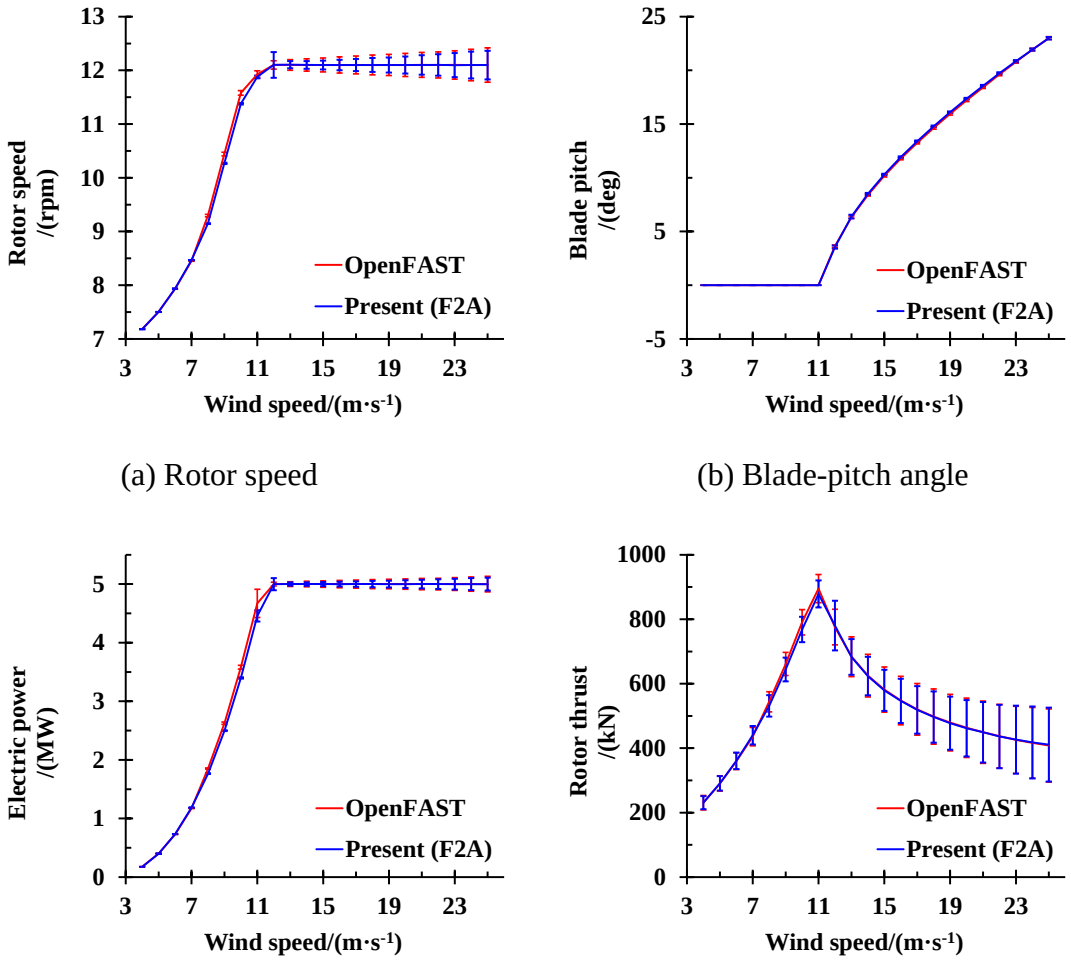

(a) Rotor speed (b) Blade-pitch angle

(c) Electric power (d) Rotor thrust

Fig. 10: Controller parameters and rotor thrust under different wind conditions

Fig. 11 compares blade dynamic responses predicted by these two tools. Fig. 11-(a) and (b) show a good agreement between F2A and OpenFAST in calculating the blade-tip deflections. Minor discrepancies of the mean deflections can be found only when the wind speed is larger than 15 m/s. Nonetheless, the difference in the standard deviation is insignificant for both out-of-plane (O-o-P) and in-plane (I-P) deflections. It implies that the fluctuation range of the blade-tip deflections predicted by F2A is close to that calculated by OpenFAST. Similar

to the results of blade-tip deflections, the blade-root bending moments obtained by F2A and OpenFAST follow the same trend versus wind speed. It is noted that the difference between the results predicted by these two tools is much smaller than that observed on blade-tip deflections for the over-rated conditions, especially the I-P bending moment. The comparison confirms that F2A is capable of predicting blade dynamics as well as OpenFAST for the FOWT under different steady wind loadings combined with regular wave loadings.

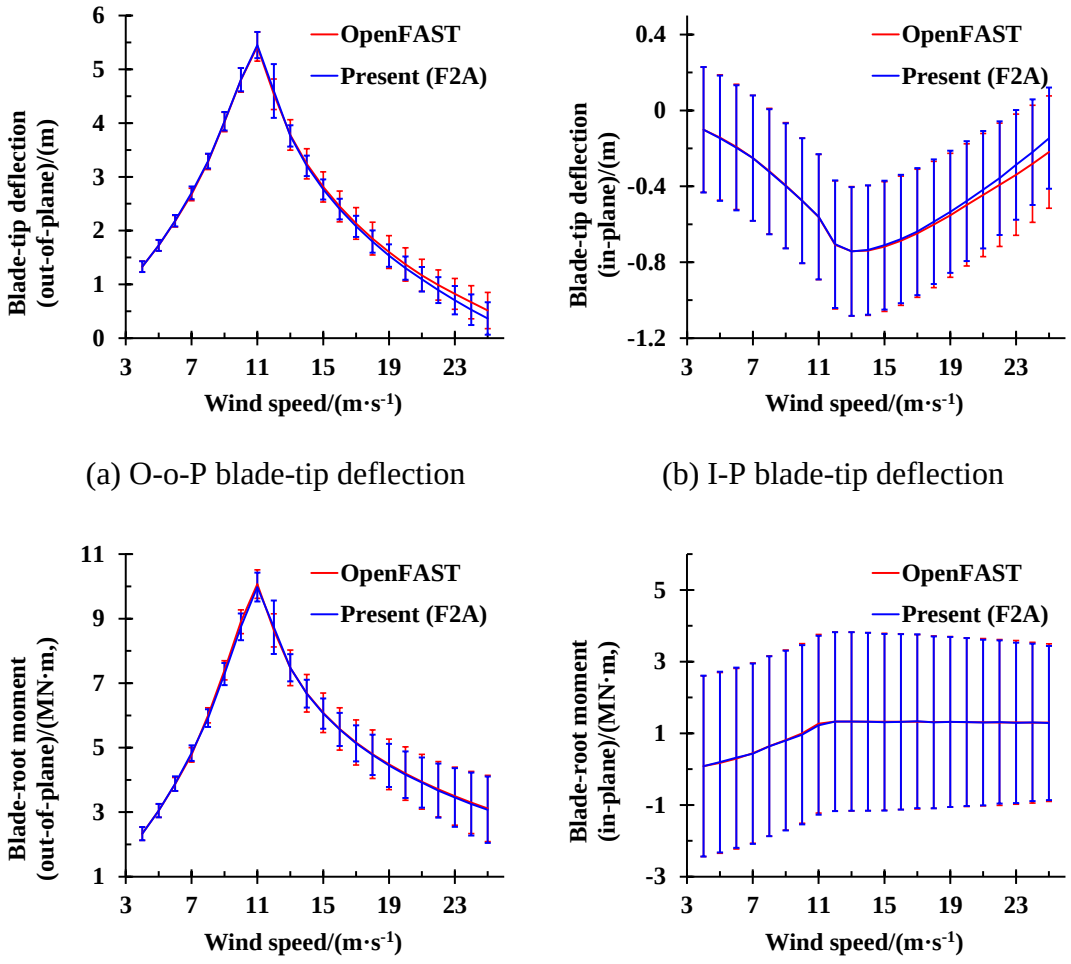

(a) O-o-P blade-tip deflection (b) I-P blade-tip deflection

(c) O-o-P blade-root moment (d) I-P blade-root moment

Fig. 11: Blade dynamic loads under different wind conditions

The tower-base loads computed using OpenFAST and F2A are compared in Fig. 12. The average magnitude and standard deviation of the tower-base force in the fore-aft direction predicted by F2A agree very well with the results produced by OpenFAST for each of the

examined DLCs. The discrepancy in the results produced by these two tools is relatively notable for the side-side force. This observation can be explained by considering the fact that the side-side force is mainly from the aerodynamic drag of blades. The aerodynamic drag is more sensitive to the local angle-of-attack (AoA) than the aerodynamic lift. A small lateral velocity from the support system will produce a notable influence on the local AoA of blade sections. It is noted that the MoorDyn module of OpenFAST employs the lumped-mass method in examining the dynamics of the mooring system. The bending stiffness of mooring lines is ignored in MoorDyn, while the finite element method is applied to examine both the axial and bending stiffness of the mooring lines in AQWA. In addition, the hydrodynamic forces acting on the mooring lines are calculated by assuming stillwater in MoorDyn, however, the wave and kinematics are coupled with the hydrodynamic load calculation of the mooring lines in AQWA. Apart from the difference of modelling mooring dynamics, minor deviations between the hydrodynamic loads in AQWA and OpenFAST could be produced due to the different excitation force obtained from the frequency-domain analysis. The differences between F2A and OpenFAST in predicting mooring dynamics and hydrodynamic loads will result in a notable discrepancy of side-side responses. Nonetheless, it is noted that the magnitude of the side-side force is less than 3% of the fore-aft force, implying that the discrepancy of the side-side force is insignificant to the resultant force.

Similar conclusions can be made on the tower-base bending moments, and the difference between the I-P tower-base bending moments obtained using the two tools is smaller than the one between the side-side forces. The discrepancy in the in-plane response moments calculated using F2A and OpenFAST is negligible compared to the resultant bending moment that is dominated by the O-o-P bending moment, in which the differences between these two tools is insignificant.

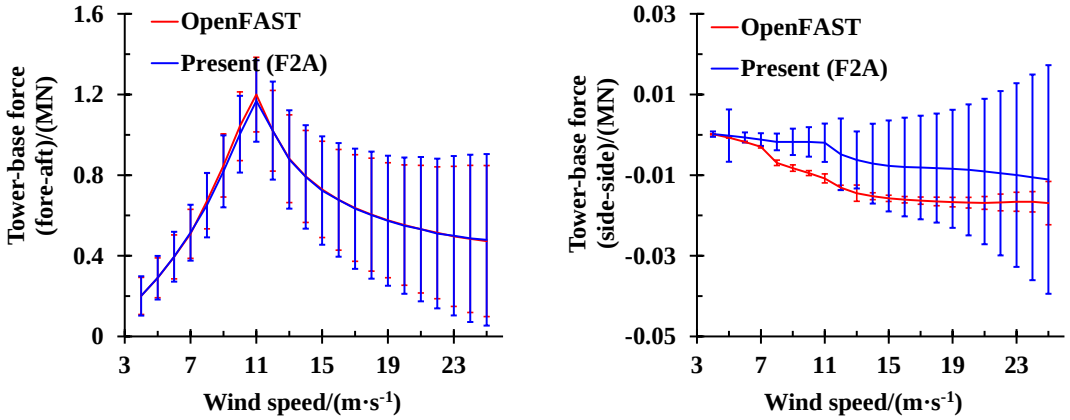

(a) O-o-P tower-base force (b) I-P tower-base force

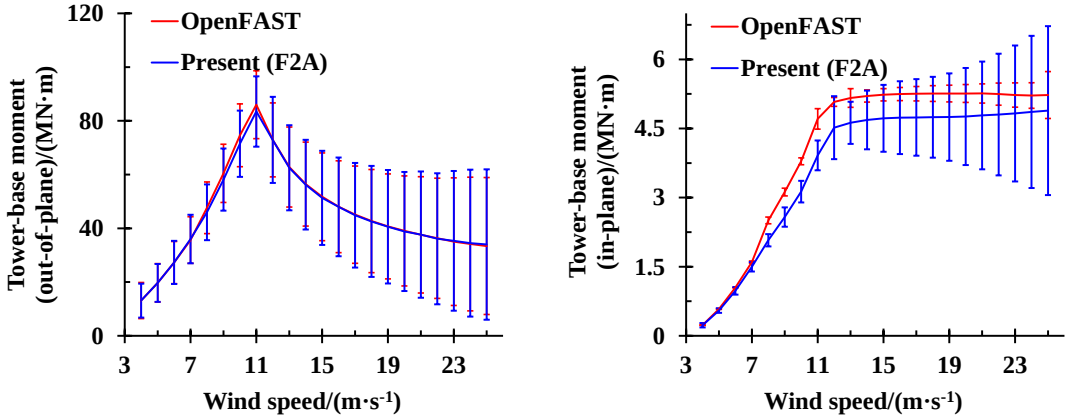

(c) O-o-P tower-base moment (d) I-P tower-base moment

Fig. 12: Tower-base loads under different wind conditions

Fig. 13 presents platform responses and mooring tensions under different conditions. It can be observed that there are good agreements between the average surge motions predicted by OpenFAST and F2A. The standard deviations corresponding to the wind speeds within 12 m /s ~ 14 m/s predicted by F2A are larger than those calculated by OpenFAST. The platform pitch predicted by F2A is almost the same as the result calculated by OpenFAST for all of the examined DLCs, though slight differences with a maximum value of 3.8% can be observed for the wind speeds close to 11 m/s. It is noted that the standard deviations of the pitch motion calculated by F2A and OpenFAST agree very well. The agreements of the platform responses validate the accuracy of F2A in predicting fully-coupled responses of a FOWT.

Fig. 13- (c) and (d) show good agreements between the fairlead tensions of the mooring lines calculated using F2A and OpenFAST for both the average value and standard deviation. One relative large discrepancy of the standard deviation is observed for the condition with a wind speed of 13 m/s. It implies that the tension predicted using F2A fluctuates in a relative larger range due to the modelling difference of mooring dynamics between AQWA and OpenFAST. Nonetheless, the relative errors between the fairlead tension calculated by F2A and OpenFAST are acceptable for the remaining DLCs.

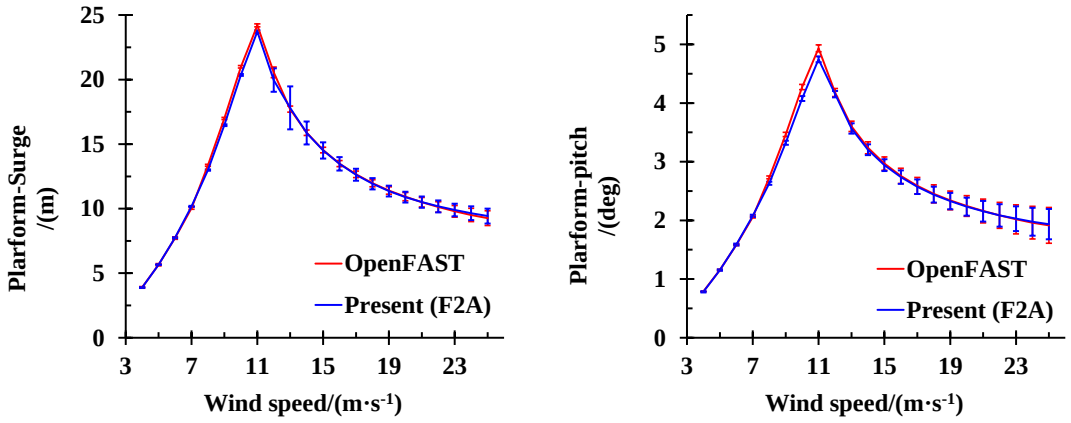

(a) Platform-surge (b) Platform-pitch

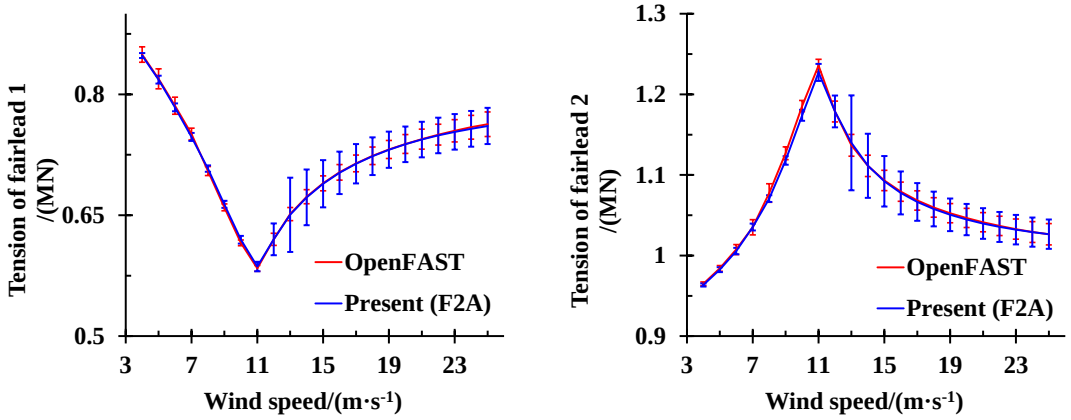

(c) Tension of fairlead 1 (d) Tension of fairlead 2

Fig. 13: Platform responses and mooring tensions under different wind conditions

3.2.4 Turbulent wind conditions

The validation against OpenFAST is enhanced by comparing the time-varying responses under turbulent wind conditions. The full-field turbulent wind generated using TurbSim based on the Kaimal spectrum is presented in Fig. 14. The average speed at the hub-height is 11.4 m/s and the power-law exponent of the vertical wind profile is 0.12. The corresponding wave height and period of the regular wave are 1.94 m and 5.01 s, respectively. The simulation has a duration of 4000 s and a time-step of 0.005 s.

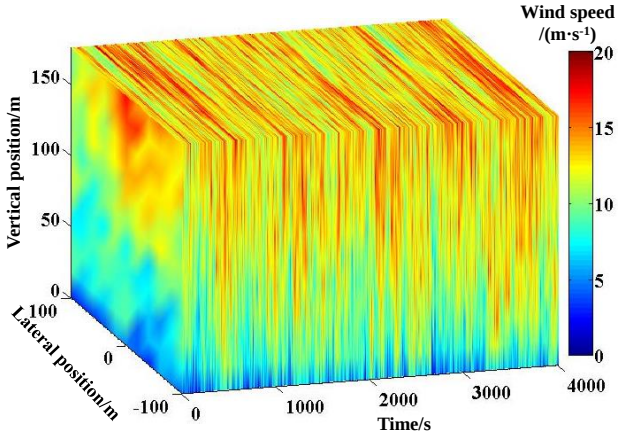

Fig .14: Turbulent wind field with an average speed of 11.4 m/s at the hub-height

Fig. 15 presents the blade-pitch, rotor speed and electric power predicted in OpenFAST and F2A. The variations of blade-pitch angle calculated by F2A agree very well with those results obtained from OpenFAST over the entire simulation, despite the minor differences at some turning points. The agreement between the rotor speeds calculated by these tools is even better than the one for the blade-pitch angle. The rotor speed predicted by F2A follows the same trend as the result of OpenFAST. Moreover, the mismatch can only be observed for a few time moments. The agreement in the electric power variations between F2A and OpenFAST is as good as that corresponding to blade pitch, though slight inconsistences between the results obtained using F2A and OpenFAST exist at power spikes. The results presented in Fig. 13 indicate that the servo-control capability has been well integrated with AQWA through the developed coupling framework F2A.

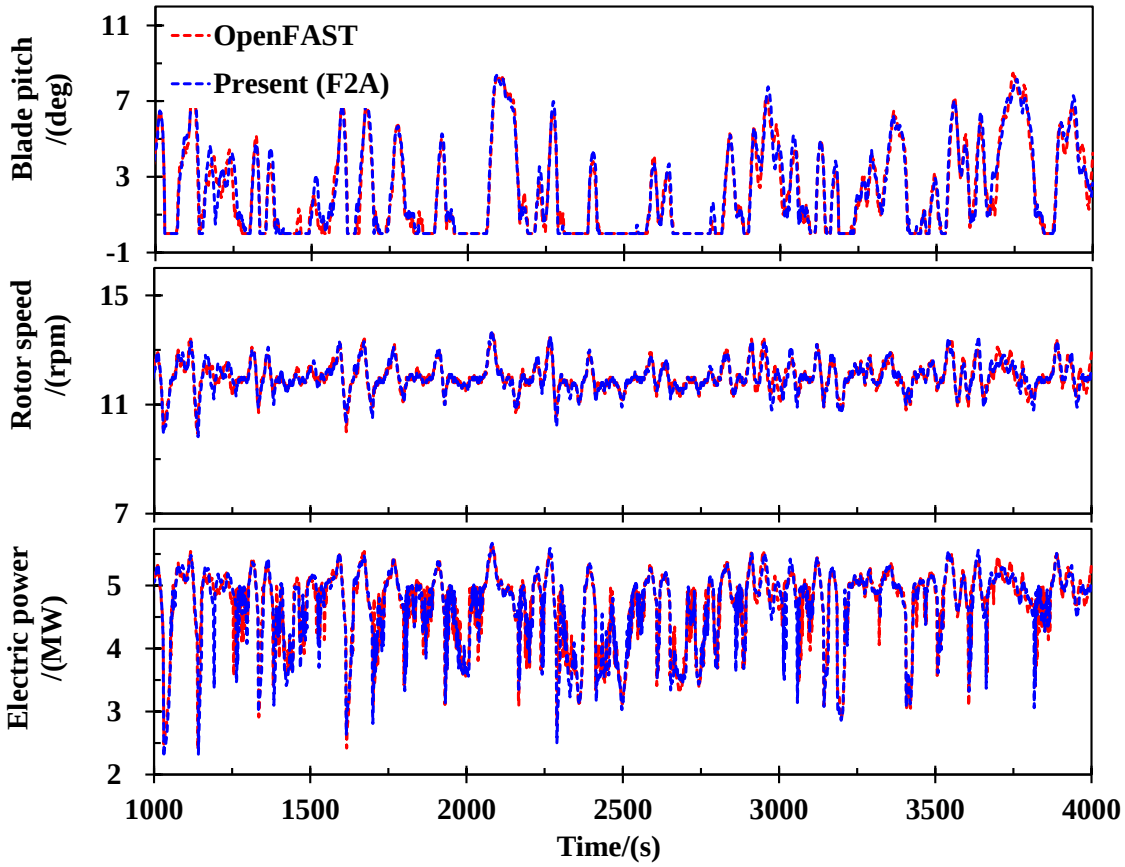

Fig. 15: Blade-pitch, rotor speed and electric power under the turbulent wind condition

The blade-tip deflections under the turbulent wind condition calculated by F2A and OpenFAST are presented in Fig. 16. The variation of the O-o-P blade-tip deflection obtained using F2A has the same trend as the results calculated by OpenFAST over the simulation length. In addition, the discrepancy in magnitude between the results obtained by these two tools is insignificant. From the locally enlarged view of the result during the period from 2500 s to 2600 s, the results predicted by these two tools have the same variation trend though the magnitudes do not well match at each time-step. Nonetheless, the difference in such magnitudes is minor. The agreements between the I-P blade-tip deflections calculated by F2A and OpenFAST are excellent, since one of the two lines can be treated as the other one with a phase shift and minor magnitude difference. The comparison indicates that the capability of predicting aero-elastic responses of the wind turbine has been well implemented within AQWA

through the developed coupling framework.

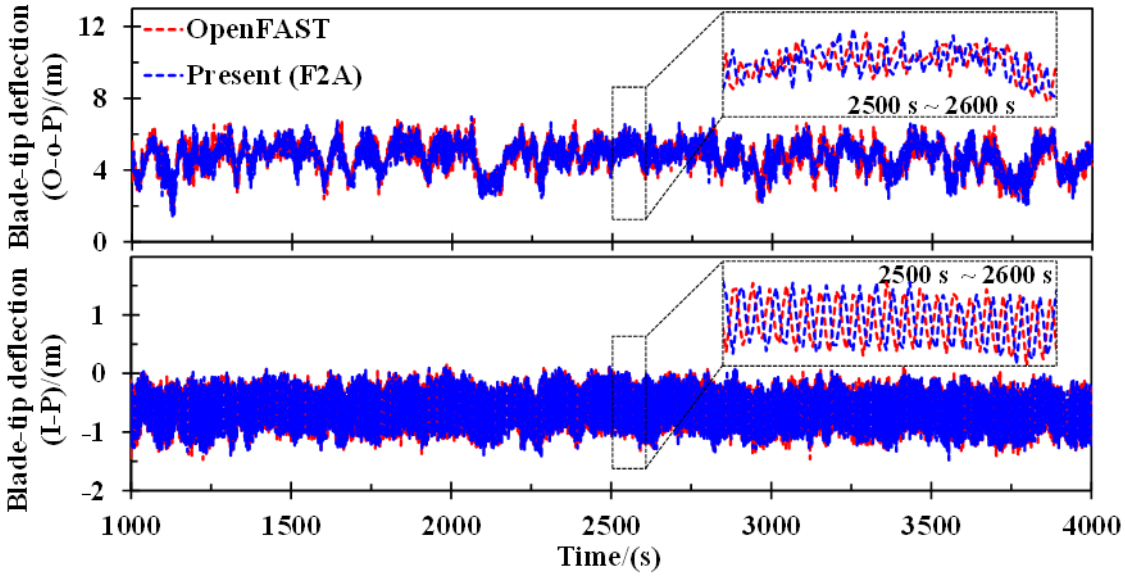

Fig. 16: Blade-tip deflections under the turbulent wind condition

Fig. 17 presents the comparison between the tower-base bending moments of F2A and OpenFAST. F2A has a good agreement with OpenFAST in predicting the O-o-P bending moment. The time-domain variations have the same trend and similar magnitudes. The comparison between the O-o-P tower-base bending moments within the period from 2500 s to 2600 s indicates that the result of F2A varies in the same frequency with a slightly smaller magnitude and a fixed phase-shift to the result of OpenFAST. The discrepancy between the torsional tower-base bending moments obtained by these two tools is even smaller than the one of the O-o-P responses. It is noted that notable differences can be observed from the I-P tower-base bending moment, nevertheless, the average value is close. The existence of the discrepancies can be explained by considering that there are differences between AQWA and OpenFAST in predicting the hydrodynamic loads and mooring restoring forces. As discussed previously, the I-P bending moment is mainly contributed by the aerodynamic drag that is heavily influenced by the lateral kinematics of the wind turbine. Hence the difference in modelling mooring dynamics using the two tools may result in a notable discrepancy on the I-

P responses. Nonetheless, F2A has an excellent agreement with OpenFAST in predicting the O-o-P bending moment that is the main contribution to the resultant bending moment at the tower-base. To be more specific, the maximum resultant bending moments predicted by F2A and OpenFAST are 127.70 MN·m and 127.85 MN·m, while the difference between the maximum I-P bending moments predicted by these two tools is around 4.23 MN·m, giving an equivalent error of 3.31% that falls within a well acceptable range in design of FOWTs. The comparison of tower-base loads confirms that FAST has been well incorporated with AQWA to predict fully-coupled dynamic responses of a FOWT.

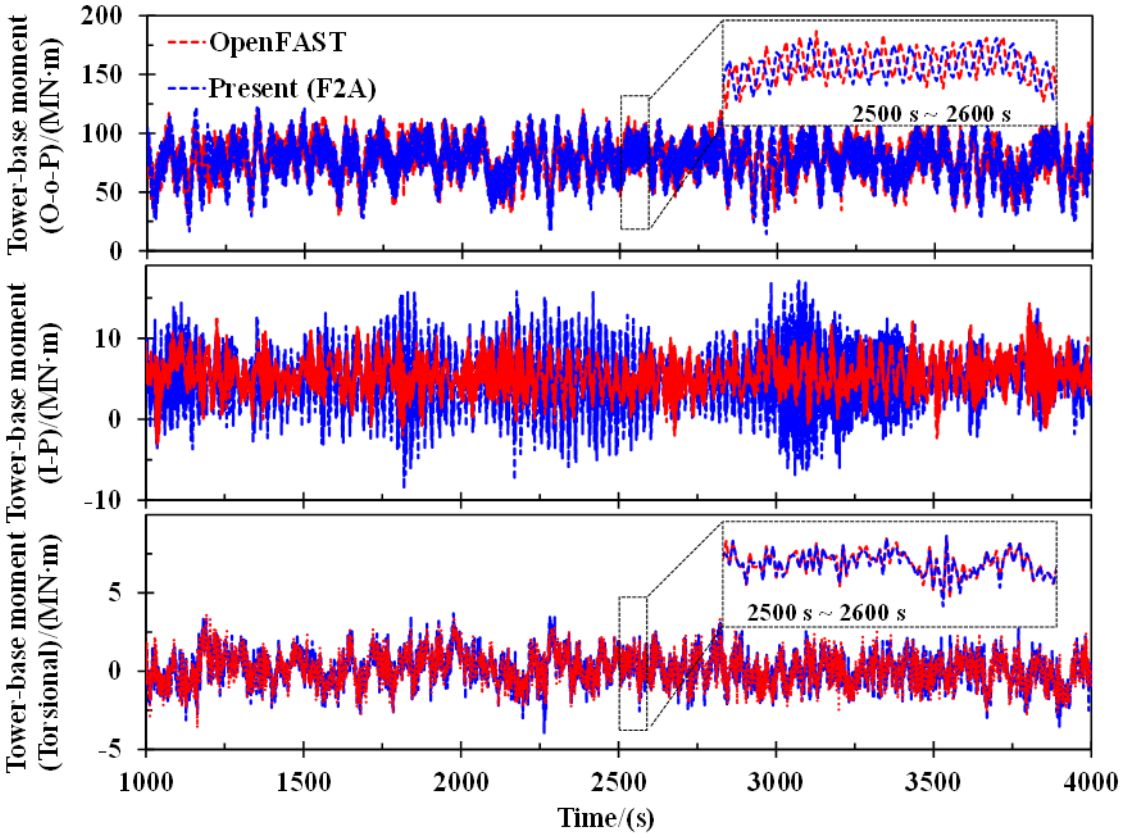

Fig. 17: Tower-base bending moments under the turbulent wind condition

Fig. 18 presents the fairlead tensions of the mooring lines calculated using F2A and OpenFAST. It is found that the variation trends of the tensions predicted by these two tools have a good agreement. The tension predicted by F2A fluctuates at a relatively larger range

before 2000th s for each of the mooring lines. However, the degree of discrepancy decreases gradually along with the completion of the transient behavior of the platform. It is found that the tension predicted by F2A follows the same trend and similar fluctuation with the result obtained in OpenFAST after 2500th s. It is noted that transient behaviors of the blades or tower last less than 1000 s that is much shorter than the transient duration of the mooring system. The reason is that the mooring dynamics are associated with the platform that has much larger natural periods than the upper structures. As a result, the transient behaviors would last longer. Another reason is that there are differences between AQWA and OpenFAST in examining dynamics of the mooring system and hydrodynamic loading. To be more specific, the MoorDyn module in OpenFAST employs the lumped-mass method to model the mooring lines. The bending stiffness of each mooring line is not considered. However, the finite element method is used in AQWA to consider both the axial and bending stiffness of the mooring lines. In addition, the hydrodynamic forces acting on the mooring lines are calculated by assuming a stillwater in MoorDyn, while the wave and current kinematics are coupled with the hydrodynamic load calculation of the mooring lines in AQWA. The difference between the hydrodynamics from HydroDyn in OpenFAST and AQWA is mainly caused by the difference of excitation forces obtained from the frequency-domain analysis. As required by HydroDyn, the vertical center of mass of the platform is set to zero when performing the frequency-domain analysis using WAMIT in order to avoid double counting the pitch/roll restoring force since the ElastDyn module in OpenFAST intrinsically accounts for these terms if the platform weight and center of mass location are appropriately defined. Consequently, the excitation pitch force used in OpenFAST is smaller as presented in Fig. 8. These differences between AQWA and OpenFAST in terms of the modelling of hydrodynamics and mooring system are the main contributors to the differences observed in Fig. 18.

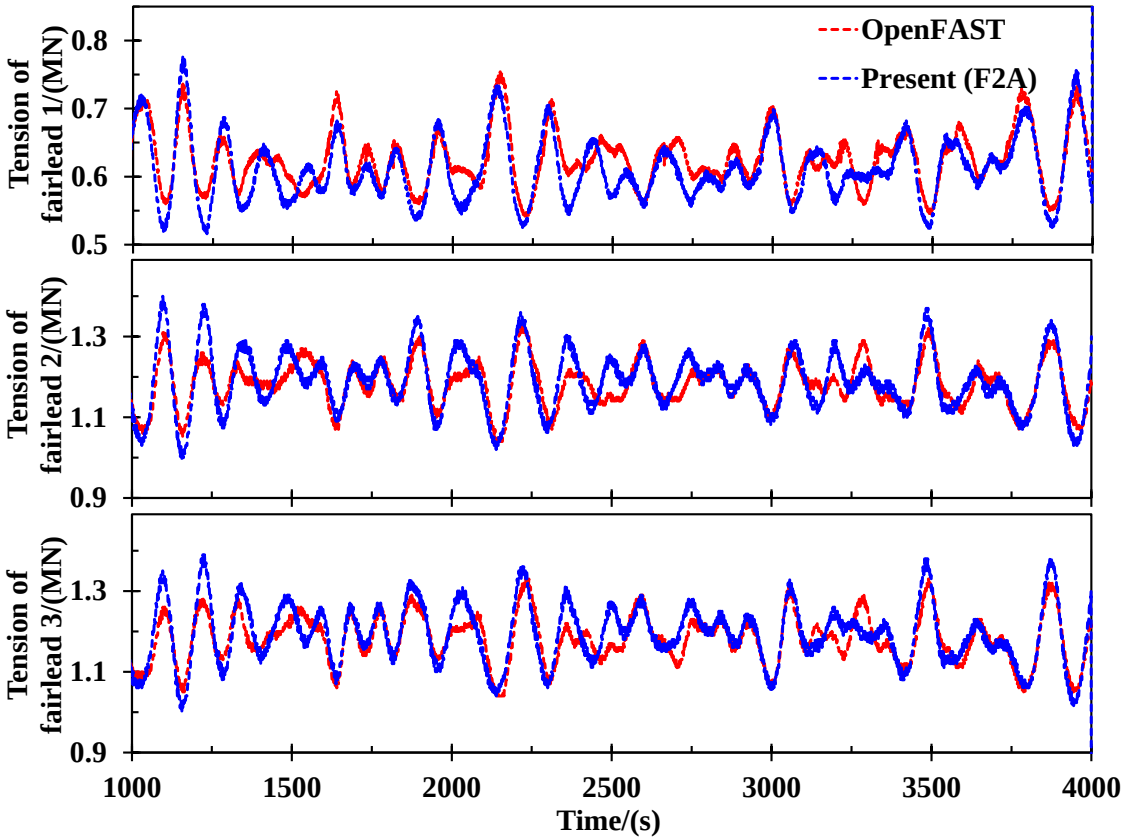

Fig. 18: Fairlead tensions of the mooring lines under the turbulent wind condition

Fig. 19 presents the comparison between platform motions predicted using OpenFAST and F2A. It is found that the magnitude and variation of the platform pitch predicted using F2A agree well with the results obtained by OpenFAST. The misalignment between the heave motions calculated by these two tools over the simulation is minor. The surge motion predicted by F2A has the same variation trend as the result of OpenFAST. Notable discrepancies between the surge motions predicted by these two tools can be observed before 2000th s. The degree of discrepancy decreases gradually and disappears at the completion of the transient behavior in the surge direction. As can be observed from the results after 2500th s, the agreement between the surge motions is excellent in terms of both the variation trend and magnitude fluctuation. The discrepancy between the surge motions predicted by these two tools is mainly due to the difference of mooring dynamics, which produces a notable influence on the transient behavior

of the platform. As discussed previously, the surge period of the platform is much larger than the periods in heave and pitch directions. Consequently, the process of the transient behavior requires a longer duration. In addition, the influence of the differences of mooring dynamics and hydrodynamic loads disappears gradually. Therefore, the results after 2500th s show very good agreements between these two tools for the surge motion.

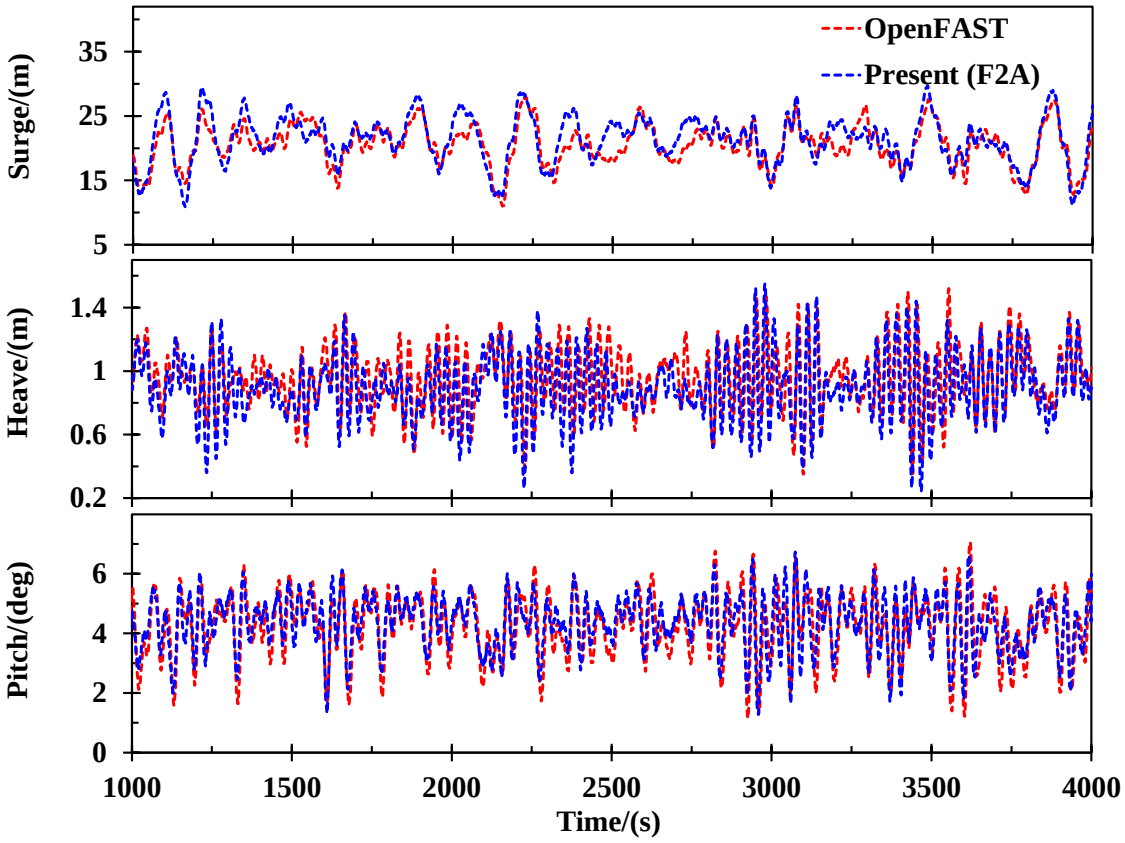

Fig. 19: Platform motions under the turbulent wind condition

Overall, the comparisons presented above have validated that F2A is capable of accurately predicting fully-coupled responses of a FOWT under steady and turbulent wind conditions. The discrepancies of the platform surge and fairlead tension of mooring lines observed before the completion of the transient behaviors fall within an acceptable range. For the results after the transient period, the coupled responses including platform surge and fairlead tensions obtained using F2A and OpenFAST agree well with each other. The differences between the

results predicted by F2A and OpenFAST are mainly due to the difference in the mooring system modelling and hydrodynamic loads, which has been confirmed by the results presented in Fig. 18 and Fig. 19. The coupling framework developed in this study makes AQWA capable of performing fully-coupled analysis of FOWTs. Since AQWA has natural advantages in performing accurate hydrodynamic analysis of floaters, this study makes a significant contribution to the design of FOWTs by making AQWA to be a new and powerful tool in simulating nonlinear dynamics of FOWTs. It is not only applicable to single-body platform concepts, but also valid for conducting fully-coupled simulations for a FOWT supported by multiple floaters connected by flexible elements. A case study is presented in the next section to illustrate the unique advantage of F2A.

4 Case study: A 10 MW multi-body floating wind turbine platform

4.1 Model description of the multi-body platform

A case study is carried out for a unique multi-body 10 MW wind turbine platform. The platform consists of an upper tank and a lower tank connected by six taut steel tendons. Fig. 20 presents a schematic diagram of the 10 MW wind turbine platform. The multi-body platform concept was originally developed by ESTYCO for cost-reduction of floating wind technology using concrete. The tower is made telescopic to ease the transportation and installation processes. Further details of the platform concept can be found in [38].

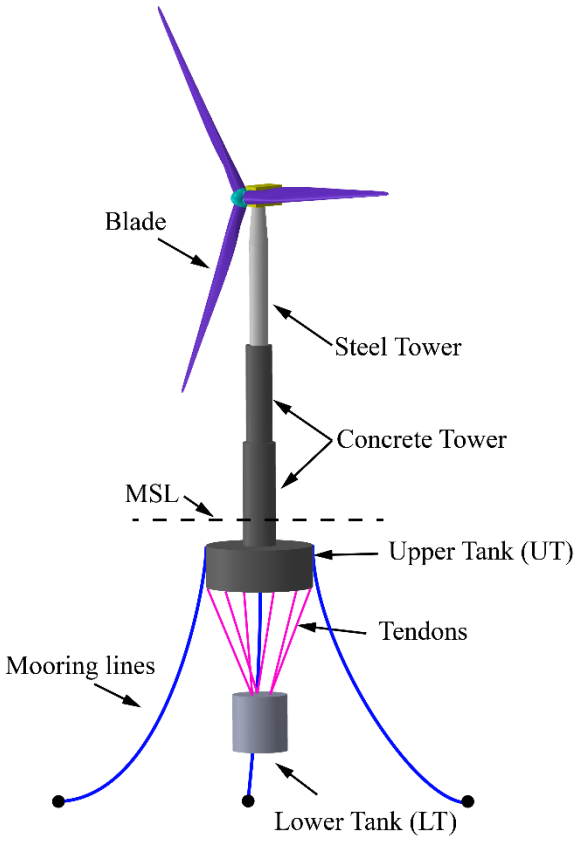

Fig. 20: Schematic diagram of the 10 MW wind turbine supported by a multi-body platform

4.2 Dynamic responses of the multi-body platform

OpenFAST in its current form is incapable of examining the dynamics of a multi-body platform. The F2A tool developed in this study addresses the limitation of OpenFAST in predicting coupled responses of a multi-body platform connected by flexible elements. In order to emphasize the necessity of modelling the platform concept as a multi-body model, the platform motions of the multi-body and unibody models subjected to wind, wave and current loadings are compared in Fig. 21, where the motions of the multi-body model are measured at the point of origin on the upper tank. For the simulation of the unibody model, the tendons are modelled as rigid elements, while each tendon is represented by a flexible steel cable in the simulation of the multi-body model. The turbulent wind has an average speed of 11.4 m/s at the hub-height. The significant wave height and spectral peak period are 1.94 m and 5.01 s,

respectively. The current speed at the MSL is 0.22 m/s.

It is observed that the surge motion of the unibody model is larger while the heave motion is slightly smaller compared to the results of the multi-body model. The difference between the pitch motions of these two models is insignificant. The reason of the large discrepancy in the surge motion of these two models is that the surge velocity perturbation due to the pitch motion of the unibody model is relatively larger since its vertical distance between the tower-base and the center of mass is longer, compared to the multi-body. Consequently, the platform motion has a larger influence on the relative inflow wind speed for the unibody model, resulting in a larger rotor thrust. The results indicate that the flexibility of the tendons cannot be ignored when investigating the dynamic behavior of the multi-body platform concept.

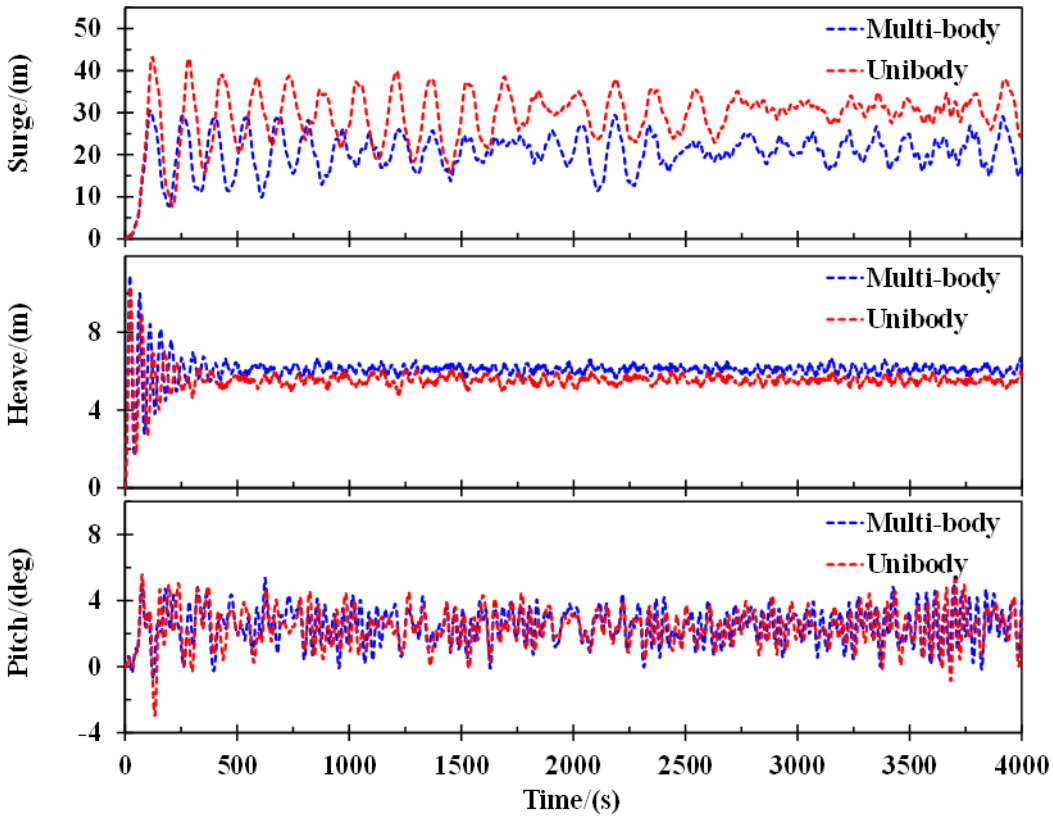

Fig. 21: Platform motions of the unibody and multi-body models

The motions of the upper and lower tanks are presented in Fig. 22. The spectral responses obtained by applying the fast Fourier transformation on the time series of the motions are

presented in Fig. 23. Although the motions of these two tanks are almost identical, slight differences are observed on the surge and pitch motions. The minor differences are induced by the local oscillation of the lower tank since the tendons are connected close to its centerline. As observed from Fig. 23, the contributions of the local pitch mode to the surge and pitch motions of the lower tank are equivalent to those of the collective pitch mode. It is apparent that this phenomenon cannot be observed from the results of a unibody. These results indicate that this unique platform concept must be modelled as a multi-body to obtain an accurate evaluation of the dynamic behaviors.

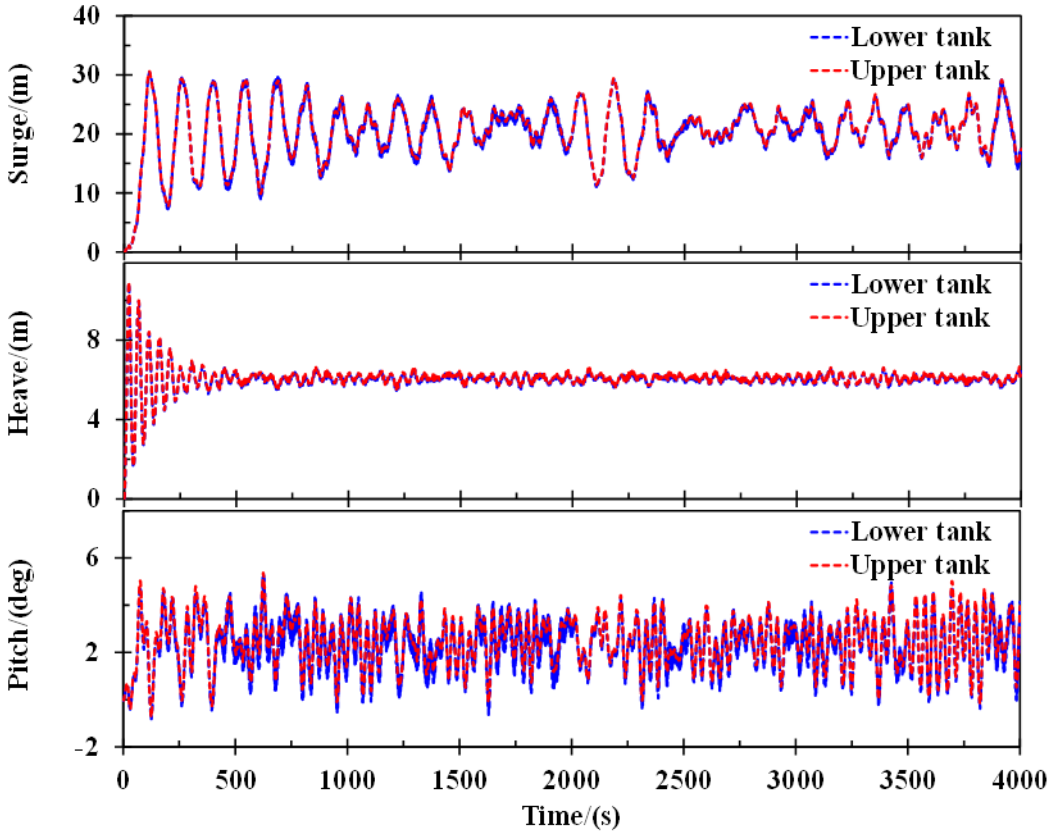

Fig. 22: Motions of the upper and lower tanks

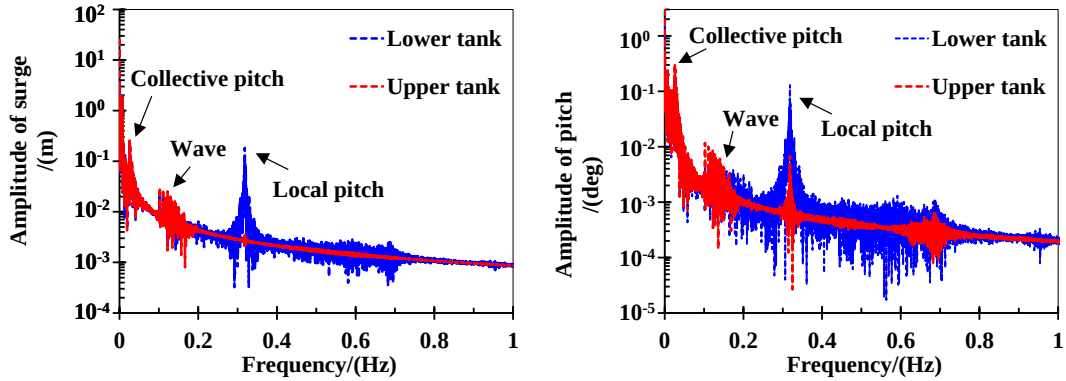

(a) Surge (b) Pitch

Fig. 23: Spectral amplitudes of the platform motions

The dynamic responses of the floating wind turbine supported by the multi-body platform can also be obtained using AQWA through a decoupled method, which means that the aerodynamic loads acting on the rotor are independent to the platform motions. In order to further emphasize the necessity of the development of F2A, the platform motions obtained through the decoupled method are compared with the results obtained using F2A in which the aerodynamic loads are coupled with the platform motions, as presented in Fig. 24. In addition, the platform motions under the wave-current condition are also presented. It is found that the platform motions under the wave-current condition are significantly smaller than the relevant results under the wind, wave and current loadings. This indicates that the wind loading must be considered in order to appropriately evaluate the dynamic behavior of the multi-body platform.

Minor differences between the surge motions obtained using the decoupled and coupled methods are observed. Similar phenomena are observed regarding the platform heave. However, certain discrepancies exist in the platform pitch motions obtained through the decoupled and coupled methods. The platform pitch motion is significantly underestimated when the coupling effects are ignored. For the coupled method, the relative wind speed is influenced by the platform surge and pitch motions, resulting in a larger fluctuation in the aerodynamic loads. Therefore, the platform pitch motion predicted using the coupled method

is larger. These results indicate that the decoupled method is incapable of appropriately evaluating the dynamic behavior of the floating wind turbine supported by the multi-body platform. This also confirms the necessity for the development of F2A.

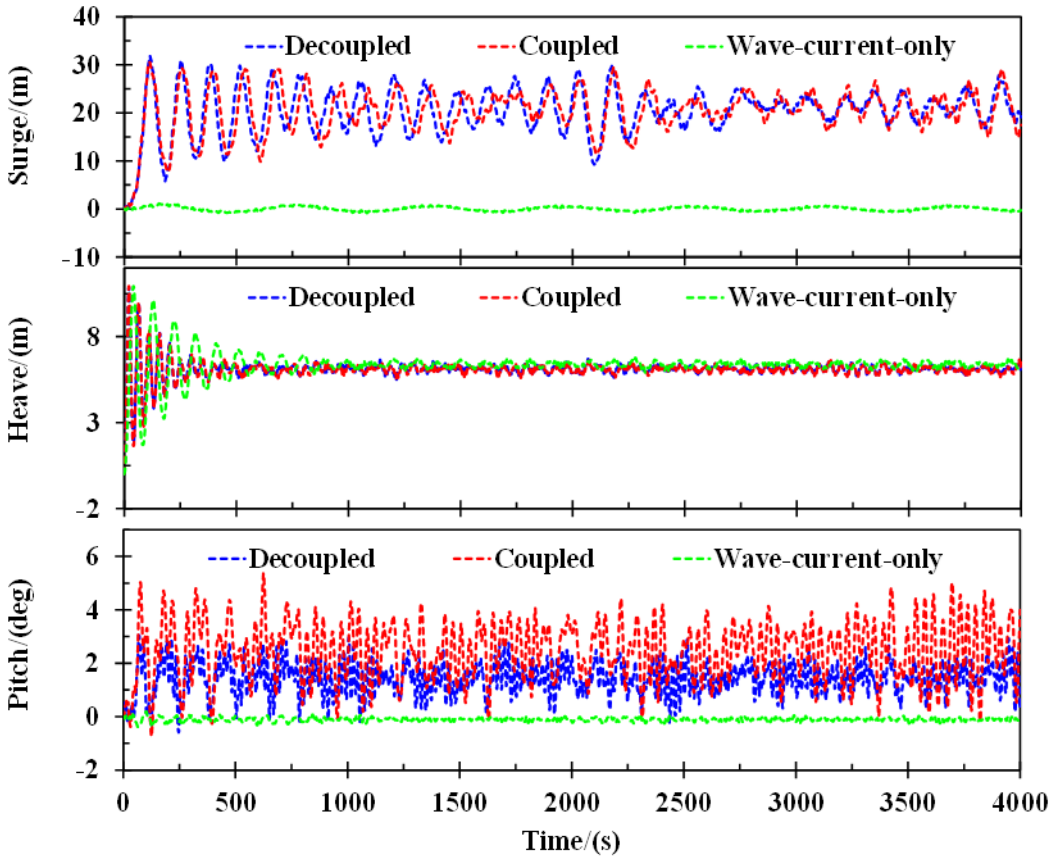

Fig. 24: Platform motions under different conditions

5 Conclusions

This study has developed a novel framework (F2A) based on FAST and AQWA to examine fully-coupled aero-hydro-servo-elastic effects of FOWTs. The implementation of F2A is achieved through modifications on source codes of the *user_force.dll* of AQWA. The aero-servo-elastic simulation capabilities are fully implemented within AQWA. The validation of F2A is carried out by comparing it with OpenFAST. The extensively-used NREL 5 MW wind turbine supported by the OC3-Hywind spar platform is employed as the validation model.

Firstly, the average values and standard deviations of the dynamic responses predicted by F2A and OpenFAST are compared under different steady wind and regular wave conditions. The comparisons show excellent agreements between the dynamic responses obtained using F2A and OpenFAST. Subsequently, time-varying dynamic responses of the FOWT subjected to the rated turbulent wind combined with a regular wave are calculated by F2A and OpenFAST and then compared. The excellent agreements in variation trend and magnitude fluctuation are observed for the dynamics of the controller, blades, tower, platform and mooring system. Although differences exist on the lateral/I-P responses of the tower, the discrepancy falls within a well-accepted level of 5%. There are natural differences between AQWA and OpenFAST in predicting hydrodynamic loads and mooring dynamics, leading to discrepancies in the platform responses and mooring tensions during the transient period. Nonetheless, it is noted that the coupled platform responses and mooring tensions predicted by these two tools agree well in magnitude variation after the transient behaviors.

The comparisons against OpenFAST have validated the accuracy of F2A in performing fully-coupled analysis of FOWTs. The natural advantages of AQWA in predicting hydrodynamic loads and mooring dynamics make F2A not only applicable to single-body platform concepts, but also valid for conducting fully-coupled simulations for a FOWT supported by multiple floaters connected by flexible elements. A case study is conducted using a unique multi-body platform. It is shown that F2A is capable of examining the interaction between the floaters of the multi-body platform. Notable differences between the platform motions are caused if the multi-body concept is simplified as a unibody. In addition, the dynamic responses obtained through a decoupled method that falls within the current capability of AQWA are significantly different from the results predicted using the coupled method. The results have confirmed the necessity for the development of F2A. These results further confirm that F2A is a powerful and necessary framework for coupled analysis of FOWTs.

Appendix A: Public release of F2A

The F2A framework is released to public on GitHub and it can be accessed via this link: https://github.com/yang7857854/F2A. The source code and a user manual of F2A have been uploaded in the repository.

Acknowledgements

This project is funded by European Regional Development Fund (ERDF), Interreg Atlantic Area (grant number: EAPA_344/2016) and the European Union's Horizon 2020 research and innovation programme under the Marie Skłodowska-Curie grant agreement no. 730888 (RESET). The authors would also like to acknowledge the financial support from Royal Society (grant number: IEC\NSFC\170054), National Natural Science Foundation of China (grant numbers: 51676131, 51976131), Science and Technology Commission of Shanghai Municipality (grant number: 1906052200)

References

[1] International Energy Agency. (2020). Offshore wind outlook 2019. World Energy Outlook Special Report.

[2] Butterfield, Sandy, Walt Musial, Jason Jonkman, and Paul Sclavounos. Engineering challenges for floating offshore wind turbines. No. NREL/CP-500-38776. National Renewable Energy Lab.(NREL), Golden, CO (United States), 2007.

[3] Le Cunff, C., Heurtier, J. M., Piriou, L., Berhault, C., Perdrizet, T., Teixeira, D. & Gilloteaux, J. C. (2013, June). Fully-coupled Floating Wind Turbine Simulator Based on Nonlinear Finite Element Method: Part I—Methodology. In *ASME 2013 32nd International Conference on Ocean, Offshore and Arctic Engineering*. American Society of Mechanical Engineers Digital Collection.

[4] Perdrizet, T., Gilloteaux, J. C., Teixeira, D., Ferrer, G., Piriou, L., Cadiou, D. & Le Cunff, C. (2013). Fully-coupled Floating Wind Turbine Simulator Based on Nonlinear Finite Element Method: Part II—Validation Results. In *ASME 2013 32nd International Conference on Ocean, Offshore and Arctic Engineering*. American Society of Mechanical Engineers Digital Collection.

[5] Chen, J., Hu, Z., Liu, G., & Wan, D. (2019). Coupled aero-hydro-servo-elastic methods for floating wind turbines. *Renewable Energy*, *130*, 139-153.

[6] Fulton, Gordon, David Malcolm, and Emil Moroz. Design of a semi-submersible platform for a 5MW wind turbine. In 44th AIAA Aerospace Sciences Meeting and Exhibit, p. 997. 2006.

[7] Beardsell, A., Alexandre, A., Child, B., Harries, R., & McCowen, D. (2018, October). Beyond OC5–Further advances in floating wind turbine modelling using Bladed. In *Journal of Physics: Conference Series* (Vol. 1102, No. 1, p. 012023). IOP Publishing.

[8] Nielsen, Finn Gunnar, Tor David Hanson, and Bjorn Skaare. Integrated dynamic analysis of floating offshore wind turbines. In 25th International Conference on Offshore Mechanics and Arctic Engineering, pp. 671-679. American Society of Mechanical Engineers, 2006.

[9] Skaare, Bjorn, Tor David Hanson, and Finn Gunnar Nielsen. Importance of control strategies on fatigue life of floating wind turbines. In ASME 2007 26th International Conference on Offshore Mechanics and Arctic Engineering, pp. 493-500. American Society of Mechanical Engineers, 2007.

[10] Jonkman, Jason M. Dynamics of offshore floating wind turbines—model development and verification. Wind Energy: An International Journal for Progress and Applications in Wind Power Conversion Technology 12, no. 5 (2009): 459-492.

[11] Jonkman, Jason Mark. Dynamics modeling and loads analysis of an offshore floating wind turbine. No. NREL/TP-500-41958. National Renewable Energy Lab.(NREL), Golden, CO (United States), 2007.

[12] Jonkman, J. M., and Denis Matha. Dynamics of offshore floating wind turbines—analysis of three concepts. Wind Energy 14, no. 4 (2011): 557-569.

[13] Li, H., Hu, Z., Wang, J., & Meng, X. (2018). Short-term fatigue analysis for tower base of a spar-type wind turbine under stochastic wind-wave loads. *International Journal of Naval Architecture and Ocean Engineering*, *10*(1), 9-20.

[14] Jahangiri, V., & Ettefagh, M. M. (2018). Multibody dynamics of a floating wind turbine considering the flexibility between Nacelle and Tower. *International Journal of Structural Stability and Dynamics*, *18*(06), 1850085.

[15] Imani, H., Abbaspour, M., Tabeshpour, M. R., & Karimirad, M. (2019). Effects of motion and structural vibration–induced loadings on the coupled dynamic response of a mono-column tension-leg-platform floating wind turbine. *Proceedings of the Institution of Mechanical Engineers, Part M: Journal of Engineering for the Maritime Environment*, 1475090219882604.

[16] Le, C., Li, Y., & Ding, H. (2019). Study on the coupled dynamic responses of a submerged floating wind turbine under different mooring conditions. *Energies*, *12*(3), 418.

[17] Han, Y., Le, C., Ding, H., Cheng, Z., & Zhang, P. (2017). Stability and dynamic response analysis of a submerged tension leg platform for offshore wind turbines. *Ocean Engineering*, *129*, 68-82.

[18] Roddier, D., Cermelli, C., Aubault, A., WindFloat: A Floating Founda-tion for Offshore Wind Turbines Part II Hydrodynamics Analysis, June 2009

[19] Kvittem, M. I., Bachynski, E. E., & Moan, T. (2012). Effects of hydrodynamic modelling in fully-coupled simulations of a semi-submersible wind turbine. *Energy Procedia*, *24*, 351-362.

[20] Michailides, Constantine, Zhen Gao, and Torgeir Moan. Experimental and numerical study of the response of the offshore combined wind/wave energy concept SFC in extreme environmental conditions. Marine Structures 50 (2016): 35-54.

[21] Shim, S. (2010). *Coupled dynamic analysis of floating offshore wind farms* (Doctoral dissertation, Texas A & M University).

[22] Bae, Y. H., Kim, M. H., & Shin, Y. S. (2010, January). Rotor-floater-mooring coupled dynamic analysis of mini TLP-type offshore floating wind turbines. In *ASME 2010 29th International Conference on Ocean, Offshore and Arctic Engineering* (pp. 491-498). American Society of Mechanical Engineers Digital Collection.

[23] Bae, Y. H., & Kim, M. H. (2013). Turbine Floater-Tether Coupled Dynamic Analysis Including Second-Order Sum-Frequency Wave Loads for a TLP-Type FOWT (Floating Offshore Wind Turbine). In *ASME 2013 32nd International Conference on Ocean, Offshore and Arctic Engineering*. American Society of Mechanical Engineers Digital Collection.

[24] Bae, Y. H., & Kim, M. H. (2014). Aero-elastic-control-floater-mooring coupled dynamic analysis of

floating offshore wind turbine in maximum operation and survival conditions. *Journal of offshore mechanics and Arctic engineering*, *136*(2).

[25] Ansys, 2010. AQWA Reference Manual Release 13.0, USA, Ansys Inc.: Canonsburg, USA.

[26] Jonkman, J. M., & Buhl Jr, M. L. (2005). Fast user's guide-updated august 2005 (No. NREL/TP-500-38230). National Renewable Energy Lab.(NREL), Golden, CO (United States).

[27] Yang, Y., Li, C., Zhang, W., Yang, J., Ye, Z., Miao, W., & Ye, K. (2016). A multi-objective optimization for HAWT blades design by considering structural strength. Journal of Mechanical Science and Technology, 30(8), 3693-3703.

[28] Moriarty, P. J., & Hansen, A. C. (2005). AeroDyn theory manual (No. NREL/TP-500-36881). National Renewable Energy Lab., Golden, CO (US).

[29] Jonkman, J. M., Hayman, G. J., Jonkman, B. J., Damiani, R. R., & Murray, R. E. (2015). AeroDyn v15 User's Guide and Theory Manual. NREL: Golden, CO, USA.

[30] Jonkman, J. M. (2003). *Modeling of the UAE Wind Turbine for Refinement of FAST_AD* (No. NREL/TP-500-34755). National Renewable Energy Lab., Golden, CO (US).

[31] Jonkman, J., & Buhl, M. (2004, January). New developments for the NWTC's fast aeroelastic HAWT simulator. In *42nd AIAA Aerospace Sciences Meeting and Exhibit* (p. 504).

[32] Newman, J. N. (2018). Marine hydrodynamics. MIT press.

[33] ANSYS, A. (2013). AQWA theory manual. ed. Canonsburg, PA 15317, USA.

[34] Jonkman, J., Butterfield, S., Musial, W., & Scott, G. (2009). *Definition of a 5-MW reference wind turbine for offshore system development* (No. NREL/TP-500-38060). National Renewable Energy Lab.(NREL), Golden, CO (United States).

[35] Jonkman, J. (2010). *Definition of the Floating System for Phase IV of OC3* (No. NREL/TP-500-47535). National Renewable Energy Lab.(NREL), Golden, CO (United States).

[36] Ifremer. Marine Data Portal, French Research Institute for the Exploitation of the Sea, Online: http://data.ifremer.fr/pdmi/portalssearch/main. Data Accessed: January 2019.

[37] Armesto, José A., Alfonso Jurado, Raúl Guanche, Bernardino Couñago, Joaquin Urbano, and José Serna. TELWIND: Numerical Analysis of a Floating Wind Turbine Supported by a Two Bodies Platform. In ASME 2018 37th International Conference on Ocean, Offshore and Arctic Engineering, pp. V010T09A073-V010T09A073. American Society of Mechanical Engineers, 2018.

[38] Yang, Y., Bashir M., Wang, J., Michailides, C., Loughney, S., Armin, M., Hernández, S., Urbano, H., and Li, C. (2020). Wind-Wave Coupling Effects on the Fatigue Damage of Tendons for a 10 MW Multi-Body Floating Wind Turbine. Ocean Engineering, In Press.